

Computing quasiconformal maps using an auxiliary metric and discrete curvature flow

Wei Zeng · Lok Ming Lui · Feng Luo ·
Tony Fan-Cheong Chan · Shing-Tung Yau ·
David Xianfeng Gu

Received: 6 October 2009 / Revised: 29 October 2011 / Published online: 3 March 2012
© Springer-Verlag 2012

Abstract Surface mapping plays an important role in geometric processing, which induces both area and angular distortions. If the angular distortion is bounded, the mapping is called a *quasiconformal mapping* (QC-Mapping). Many surface mappings in our physical world are quasiconformal. The angular distortion of a QC mapping can be represented by the Beltrami differentials. According to QC Teichmüller theory, there

T. F. Chan is supported by NSF GEO0610079, NSF IIS0914580, NIH U54RR021813 and ONR N000140910105. D. X. Gu is supported by NIH R01EB0075300A1, NSF IIS0916286, NSF CCF0916235, NSF CCF0830550, NSF III0713145, and ONR N000140910228. L.M. Lui is supported by CUHK Direct Grant (Project ID: 2060413).

W. Zeng · D. X. Gu (✉)
Department of Computer Science, Stony Brook University, Stony Brook, NY 11794, USA
e-mail: gu@cs.stonybrook.edu

W. Zeng
e-mail: zengwei@cs.stonybrook.edu

L. M. Lui
Department of Mathematics, The Chinese University of Hong Kong, Shatin, Hong Kong
e-mail: lmlui@math.cuhk.edu.hk

F. Luo
Department of Mathematics, Rutgers University, Piscataway, NJ 08854, USA
e-mail: fluo@math.rutgers.edu

T. F.-C. Chan
The Hong Kong University of Science and Technology, Kowloon, Hong Kong
e-mail: tonyfchan@ust.hk

S.-T. Yau
Department of Mathematics, Harvard University, Cambridge, MA 02138, USA
e-mail: yau@math.harvard.edu

is a one-to-one correspondence between the set of Beltrami differentials and the set of QC surface mappings under normalization conditions. Therefore, every QC surface mapping can be fully determined by the Beltrami differential and reconstructed by solving the so-called Beltrami equation. In this work, we propose an effective method to solve the Beltrami equation on general Riemann surfaces. The solution is a QC mapping associated with the prescribed Beltrami differential. The main strategy is to define an *auxiliary metric* (AM) on the domain surface, such that the original QC mapping becomes conformal under the auxiliary metric. The desired QC-mapping can then be obtained by using the conventional conformal mapping method. In this paper, we first formulate a discrete analogue of QC mappings on triangular meshes. Then, we propose an algorithm to compute discrete QC mappings using the discrete Yamabe flow method. To the best of our knowledge, it is the first work to compute the discrete QC mappings for general Riemann surfaces, especially with different topologies. Numerically, the discrete QC mapping converges to the continuous solution as the mesh grid size approaches to 0. We tested our algorithm on surfaces scanned from real life with different topologies. Experimental results demonstrate the generality and accuracy of our auxiliary metric method.

Mathematics Subject Classification (2000) 65 · 52 · 30

1 Introduction

Mapping between surfaces plays a fundamental role in digital geometry processing. In general, surface mappings introduce distortions, which can be classified as area distortion and angular distortion. Mappings without angular distortions are called conformal mappings. Last several years, there has been fast development of various techniques for computing conformal mappings and their applications in geometric processing. However, conformal mappings are not common in practice. Many mappings in our physical world are quasiconformal (QC), which introduce bounded angular distortion. For example, deformations of elastic shapes are QC, such as human expression change, deformations of human organs, etc. In order to model surface mappings in the real world more effectively, it is crucial to study QC mappings which allow for a much wider domain of applications.

The theory of QC mappings is nearly 80 years old and has been firstly studied by Ahlfors [1], Grotzsch [26], Morrey [49] and Lavrentjev [38]. QC mappings can be viewed as a generalization of conformal mappings. Figure 1 illustrates the difference between a conformal mapping and a QC mapping for a topological disk (a). Angular distortion can be characterized in the following intuitive way. Geometrically, a *conformal mapping* maps infinitesimal circles on the domain to infinitesimal circles on the image, shown as the mapping from (b) to (c). In other words, conformal mapping is angle-preserving. The conformality can be visualized by texture mapping in modern graphics. In frame (d), the checker-board texture is mapped to the surface (a) under the conformal parameterization (c). The right angles of checker-board texture in (d) are well preserved. A *quasiconformal mapping* maps infinitesimal ellipses on the domain to infinitesimal circles on the image, shown as the mapping from (e) to (f).

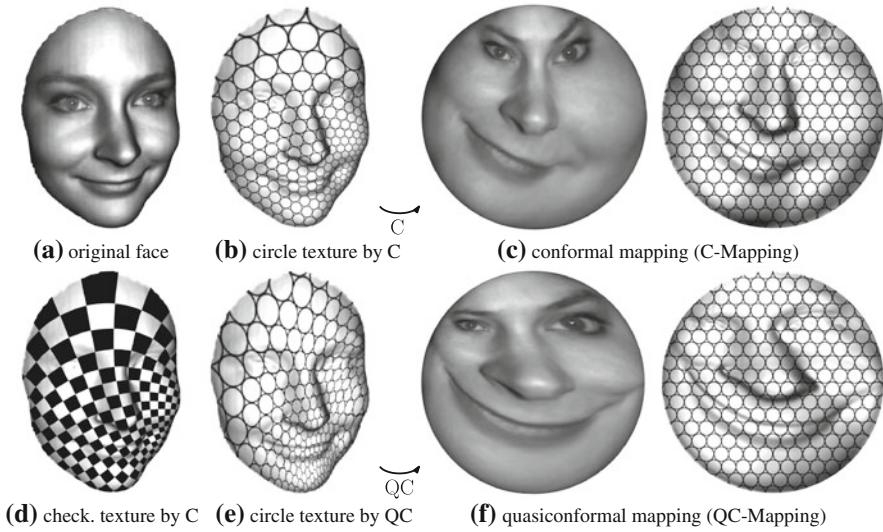
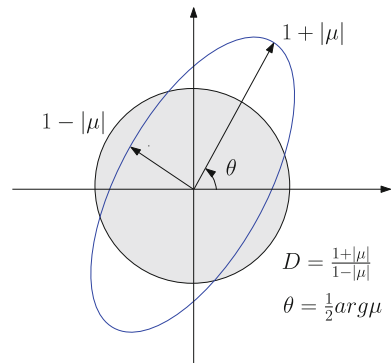


Fig. 1 Conformal and Quasiconformal mappings for a topological disk: **a** original face; **b** circle texture mapping on **(a)** induced by **(c)**; **c** conformal mapping of **(a)**; **d** checker-board texture mapping on **(a)** induced by **(c)**, visualizing the angle-preserving property of conformal mapping; **e** the circle texture mapping on **(a)** induced by **(f)**; **f** quasiconformal mapping of **(a)** associated with Beltrami differential μ . The eccentricity and orientation of ellipse demonstrate the angle distortion of quasiconformal mapping

Fig. 2 Illustration of how the Beltrami coefficient μ measures the distortion by a quasiconformal mapping that maps a small circle to an ellipse with dilation D



The eccentricity and the orientation of the ellipse can be represented by a complex valued function, the so-called *Beltrami coefficient* μ , which is defined on the surface **(a)**. Specifically, the ratio between the two axes of the ellipse is given by $\frac{1+|\mu(z)|}{1-|\mu(z)|}$, and the orientation of the axis is related to $\arg \mu(z)$ (see Fig. 2). Here, \arg is a function operating on complex numbers and it gives the angle between the line joining the point to the origin and the positive real axis, shown as θ in Fig. 2, known as an argument of the point.

Beltrami coefficient is defined on a local chart. Globally, Beltrami coefficient is represented by the *Beltrami differential*, which is independent of the choice of local parameters. According to quasiconformal Teichmüller theory, fixing any 3 points on a pair of surfaces, there is a one-to-one correspondence between the set of QC maps

and the set of Beltrami differentials. In other words, every QC mapping can be fully determined by the Beltrami differentials and is unique up to a finite dimensional group. Conversely, given a particular Beltrami differential $\mu(z)\frac{d\bar{z}}{dz}$, we can reconstruct the QC mappings associated with $\mu(z)\frac{d\bar{z}}{dz}$. The Beltrami differential captures the most essential information of the surface mappings. Therefore, by adjusting $\mu(z)\frac{d\bar{z}}{dz}$, we can reconstruct a surface mapping with desired properties.

Quasiconformal mappings have been studied extensively in complex analysis [1, 2, 26, 39]. Applications can be found in different areas such as differential equations, topology, Riemann mappings, complex dynamics as well as applied mathematics [4–7, 12, 13, 17, 42–45, 47]. Despite the rapid development in the theory of QC mapping, the progress on computing QC mappings numerically has been very slow. In fact, developing an effective numerical algorithm to compute QC mapping remains a challenging problem.

Recently, there has been a few work on numerical QC mapping techniques on the complex plane based on solving differential equations with finite difference or finite element methods. Most of these methods deal with simple domains in the complex plane and cannot be applied on arbitrary regions. Furthermore, to the best of our knowledge, no work has been done on solving the Beltrami equation on general Riemann surfaces. In this work, we are interested in developing an effective numerical algorithm to compute the QC mapping on general Riemann surfaces of any genus. The developed algorithm could be easily applied to arbitrary regions in the complex plane \mathbb{C} , since they are Riemann surfaces.

The fundamental problem in this paper is to find the QC mapping ϕ between two Riemann surfaces, associated with a given Beltrami differential. This can be done by solving the Beltrami equation using the proposed *auxiliary metric method*. We first formulate a discrete analogue of QC mappings on triangular meshes. Then, we propose a numerical algorithm to compute the discrete QC mapping. The basic idea is to construct a *discrete auxiliary metric* based on the given Beltrami differential, such that ϕ becomes a conformal mapping under the auxiliary metric. In this work, we use the discrete Yamabe flow method to compute the conformal mapping under the new discrete metric. The resulting mapping is the desired discrete QC mapping. Numerically, the discrete QC mapping converges to the continuous solution as mesh grid size tends to 0.

To the best of our knowledge, this is the first work to solve the Beltrami equation using the auxiliary metric and Yamabe flow for the purpose of computing QC mappings between two Riemann surfaces. The main contributions of this work are summarized as follows:

1. To *firstly* introduce a new concept for incorporating quasiconformality induced from Beltrami differential with a conformal structure, called the *Auxiliary Metric (AM)*.
2. To *firstly* introduce the discrete analogue of QC geometry on discrete triangular meshes using the discrete auxiliary metric. The discrete QC mapping converges to the continuous solution as mesh grid size tends to 0, which is verified both theoretically and numerically.

3. To *firstly* present a solution of computing **surface** QC mappings by solving Beltrami equation on Riemann surfaces using the auxiliary metric and the *Yamabe Flow*, called the *Quasi-Yamabe Flow*.

The paper is laid out in the following way: Sect. 2 briefly reviews the most related works in the field; Sect. 3 introduces the smooth theoretical background for QC mapping and explains how the Beltrami equation can be solved on general Riemann surfaces using the auxiliary metric; Sect. 4 describes the discrete analogue of QC geometry on triangular meshes; Sect. 5 focuses on the computational methodologies of the proposed discrete Quasi-Yamabe flow; Sect. 6 shows the numerical proof of the convergence of the proposed algorithm; Sect. 7 reports the experimental results; the paper is concluded in Sect. 8.

2 Previous work

Recently, there has been various work on numerical QC mapping techniques based on solving elliptic equations in the real plane with finite difference or finite element methods. Using finite difference methods to compute QC mappings on complex plane were proposed by Belinskii et al. [12] and Mastin and Thompson [47]. These methods are difficult to implement for arbitrary regions. A finite difference scheme for constructing QC mappings for arbitrary simply and doubly-connected region of the plane onto a rectangle was developed by Mastin and Thompson [48]. Vlasynk [56] applied similar techniques for mappings of doubly connected and triply connected domains onto a parametric rectangle. A finite element based method was implemented by Weisel [58] for computing the modulus of quadrilaterals. In [18] Daripa proposed a numerical construction of QC mappings in the plane using the Beltrami equation. The author presented an algorithm for the evaluation of one of the singular operators that arise in solving the Beltrami equation. The author subsequently applied the same method for numerical QC mappings of the exterior of simply connected domains onto the interior of a unit disk using the Beltrami equation [17]. This method was further extended to the QC mapping of an arbitrary doubly connected domain with smooth boundaries onto an annulus $\Omega_R = \{\sigma : R < \sigma < 1\}$ [19]. All of these methods deal with simple domains in the complex plane and cannot be applied on arbitrary regions. Furthermore, to the best of our knowledge, no work has been done on solving the Beltrami equation on general Riemann surfaces with arbitrary topologies.

In recent decade, there is solid theoretical progress on conformal mapping. Circle pattern was proposed by Bowers and Hurdal [10], and has been proven to be a minimizer of a convex energy by Bobenko and Springborn [9]. An efficient circle pattern algorithm was developed by Kharevych et al. [36]. Discrete Ricci flow based on circle packing method was introduced by Chow and Luo [15] and applied to graphics in [35]. The other efficient method for scaling metrics to prescribed curvatures was introduced in [3]. As the surface curvature flow methods, the smooth Yamabe flow and the smooth Ricci flow are equivalent. However, their numerically computational algorithm are different due to their different discretization solution. The theory for combinatorial Euclidean Yamabe flow was introduced by Luo [46]. The theory for hyperbolic case was introduced in [8]. Springborn et al. [55] identified the Yamabe

energy with the Milnor–Lobachevsky function and the heat equation for the curvature evolution with the cotangent Laplace equation. Gu et al. [60] developed the discrete Yamabe flow algorithm for computing arbitrary high-genus surfaces.

Conformal mapping has been broadly applied to surface parameterizations in digital geometry processing. Here we only review the most related work. We refer readers to the thorough surveys of [22, 34, 53] for various kinds of mesh parameterization techniques. Lévy et al. [40] applied the Cauchy–Riemann equation for mesh parameterization and provided successful results on the constrained 2D parameterizations with free boundaries. Desbrun et al. [20] minimized the Dirichlet energy defined on triangular meshes for computing conformal parameterization. Sheffer et al. [52, 54] introduced the angle based flattening (ABF) method. Zayer et al. [59] presented the linearized version of ABF. Gu and Yau [29] computed the conformal structure using Hodge theory and holomorphic 1-form. Gortler et al. [23] applied discrete 1-forms for mesh parameterization with several holes. Ray et al. [51] used holomorphic 1-form to follow the principle curvatures for the quad remeshing purpose. Kälberer et al. [37] introduced branched covering to convert a given frame field on the surface to a vector field on the covering space. In addition, spherical parameterizations were introduced in [24, 50]. High genus surface parameterization was pioneered by Grimm and Hughes in [25]. Recently, hyperbolic parameterization was introduced for high genus surfaces in [35]. Conformal mapping has also been widely used in the engineering fields, such as brain morphology study [28], colon flattening [33], and supine-prone colon registration [61] in medical imaging, manifold spline [27] in geometric modeling, shape analysis, shape matching and registration [41, 57, 62, 63] in computer vision, and so on.

3 Smooth quasiconformal theory

In this section, we briefly introduce the major concepts in differential geometry, Riemann surface theory and conformal geometry, which are necessary to explain the QC mappings. We refer readers to [21, 30] for detailed information. We further present the main theorem of this work, which founds the computational background for QC mappings by solving Beltrami equation using the auxiliary metric. The symbols used for presentation are listed in Table 1.

3.1 Conformal geometry

Let $\omega = f(z) : \mathbb{C} \rightarrow \mathbb{C}$ be a complex function. The following differential operators are convenient for the discussion

$$\frac{\partial}{\partial z} := \frac{1}{2} \left(\frac{\partial}{\partial x} - i \frac{\partial}{\partial y} \right), \quad \frac{\partial}{\partial \bar{z}} := \frac{1}{2} \left(\frac{\partial}{\partial x} + i \frac{\partial}{\partial y} \right).$$

f is said to be *quasiconformal* associated with μ if it is orientation-preserving and satisfies the following *Beltrami equation*:

Table 1 Symbol list

S	Smooth surface	M	Triangular mesh
μ	Beltrami coefficient	v_i	i th vertex
z, w	Isothermal coordinates	$[v_i, v_j]$	Edge connecting v_i and v_j
f	General surface mapping	g_{ij}	Riemannian metric on $[v_i, v_j]$
U_α, V_β	Neighborhoods on S	u_i	Conformal factor on v_i
ϕ_α, ψ_β	Coordinates mapping	l_{ij}	Edge length on $[v_i, v_j]$
(U_α, ϕ_α)	Isothermal coordinate chart	L_{ij}	Conformal deformation of l_{ij}
$\phi_{\alpha\beta}$	Holomorphic coordinates transition	θ_i	Corner angle on v_i
$f_{\alpha\beta}$	QC coordinates transition	μ_{ij}	Beltrami coefficient on $[v_i, v_j]$
K	Gaussian curvature	l	Discrete metric (edge length)
\bar{K}	Target curvature	\tilde{l}	Discrete auxiliary metric
\mathbf{g}	Riemannian metric	Γ	Lattice of universal covering space
\mathbf{u}	Conformal factor	H	Hessian matrix

$$\frac{\partial f}{\partial \bar{z}} = \mu(z) \frac{\partial f}{\partial z},$$

where $\mu(z)$ is some complex-valued Lebesgue measurable function satisfying $\sup |\mu| < 1$. μ is called the *Beltrami coefficient* of f . The Beltrami coefficient μ gives us all the information about the conformality of f (see Fig. 2). If $\mu(z) = 0$ everywhere, f is called *holomorphic*. A holomorphic function satisfies the well-known Cauchy–Riemann equation

$$\frac{\partial f}{\partial \bar{z}} = 0.$$

Suppose S is a surface embedded in \mathbb{R}^3 , with the induced Euclidean metric \mathbf{g} . Let $U_\alpha \subset S$ be an open set on S , with local parameterization $\phi_\alpha : U_\alpha \rightarrow \mathbb{C}$, such that the metric has local representation

$$\mathbf{g} = e^{2\lambda(z)} dz d\bar{z},$$

where $\lambda(z)$ is called conformal factor, denoting the area distortion under ϕ_α . Then (U_α, ϕ_α) is called an *isothermal coordinate chart*. We can cover the whole surface by a collection of isothermal coordinate charts. All isothermal coordinate charts form a *conformal atlas*. The maximal conformal atlas is a *conformal structure*. The surface with a conformal structure is called a *Riemann surface*.

Suppose S_1 and S_2 are two Riemann surfaces. (U_α, ϕ_α) is a local isothermal chart of S_1 , (V_β, ψ_β) is a local chart of S_2 . $f : S_1 \rightarrow S_2$ is a *conformal mapping* if and only if

$$f_{\alpha\beta} = \psi_\beta \circ f \circ \phi_\alpha^{-1} : \phi_\alpha(U_\alpha) \rightarrow \psi_\beta(V_\beta)$$

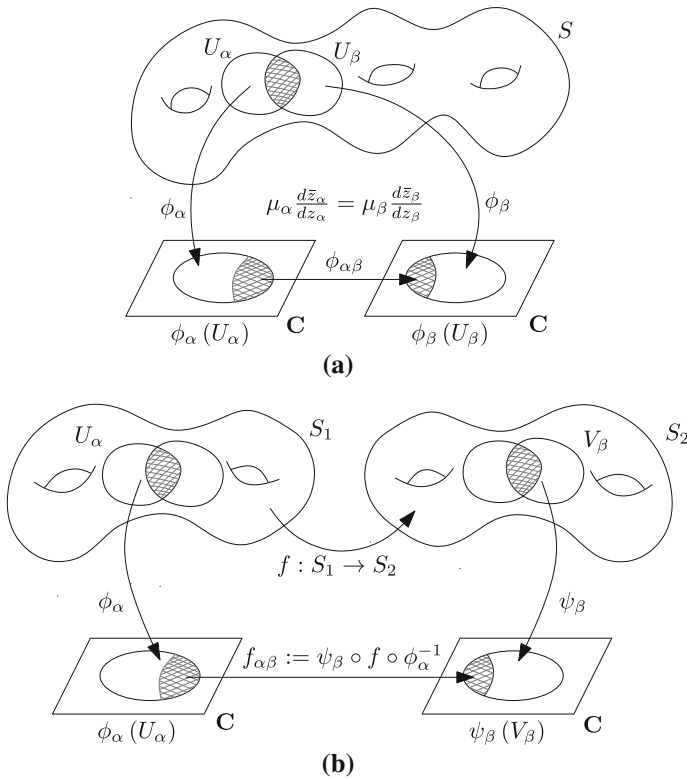


Fig. 3 Beltrami differential and quasiconformal mapping between Riemann surfaces. **a** Beltrami differential on Riemann surface. **b** mapping between Riemann surfaces

is bi-holomorphic for all ϕ_α and ψ_β . For simplicity, we still use f to denote its local representation. Then a conformal mapping f satisfies $\frac{\partial f}{\partial \bar{z}} = 0$. The geometric illustration is shown in Fig. 3.

3.2 Quasiconformal mapping

The definition of QC mappings of plane domains can be extended to Riemann surfaces. Instead of using the Beltrami coefficient, a global quantity called *Beltrami differential* is used, which is independent of the choice of local parameters.

Definition 3.1 (Beltrami Differential) A *Beltrami differential* $\mu(z) \frac{d\bar{z}}{dz}$ on a Riemann surface S is an assignment to each chart (U_α, ϕ_α) of an L_∞ complex-valued function μ_α , defined on local parameters z_α , such that

$$\mu_\alpha(z_\alpha) \frac{d\bar{z}_\alpha}{dz_\alpha} = \mu_\beta(z_\beta) \frac{d\bar{z}_\beta}{dz_\beta} \tag{1}$$

on the domain which is also covered by another chart (U_β, ϕ_β) , where $\frac{dz_\beta}{dz_\alpha} = \frac{d}{dz_\alpha} \phi_{\alpha\beta}$ and $\phi_{\alpha\beta} = \phi_\beta \circ \phi_\alpha^{-1}$.

Basically, if a surface is covered by only one coordinate chart, we can use one Beltrami coefficient defined on that chart to describe the QC mapping. However, in case the surface is covered by more than one chart, several Beltrami coefficients defined on each chart are required to represent the QC mapping. In this case, the collection of these Beltrami coefficients is called the Beltrami differential. The Beltrami differential has to satisfy the consistency condition on the overlapping regions of different charts, so that the definition is well-defined.

Now a QC mapping between Riemann surfaces can be defined as follows (see Fig. 3 for the geometric illustration):

Definition 3.2 (*Quasiconformal Mapping between Riemann Surfaces*) An orientation preserving homeomorphism $f : S_1 \rightarrow S_2$ is called *quasiconformal* associated with $\mu \frac{d\bar{z}}{dz}$ if for any chart (U_α, ϕ_α) on S_1 and any chart (V_β, ψ_β) on S_2 , the mapping $f_{\alpha\beta} := \psi_\beta \circ f \circ \phi_\alpha^{-1}$ is QC associated with $\mu_\alpha(z_\alpha) \frac{d\bar{z}_\alpha}{dz_\alpha}$.

Note that the above definition is well defined. On a region of S_1 covered by two different charts z_α and $z_{\alpha'}$. We have $\frac{dz_\alpha}{dz_{\alpha'}} = 0$, therefore

$$\mu_{\alpha'}(z_{\alpha'}) = \frac{\partial f_{\alpha'\beta}}{\partial \bar{z}_{\alpha'}} \Big/ \frac{\partial f_{\alpha'\beta}}{\partial z_{\alpha'}} = \left(\frac{\partial f_{\alpha\beta}}{\partial \bar{z}_\alpha} \frac{d\bar{z}_\alpha}{dz_{\alpha'}} \right) \Big/ \left(\frac{\partial f_{\alpha\beta}}{\partial z_\alpha} \frac{dz_\alpha}{dz_{\alpha'}} \right) = \mu_\alpha(z_\alpha) \frac{d\bar{z}_\alpha}{dz_{\alpha'}} \Big/ \frac{dz_\alpha}{dz_{\alpha'}}. \tag{2}$$

This is guaranteed by Eq. (1). Also, the definition does not depend on the chart w_β used in the range of f . Let w_β and $w_{\beta'}$ be two different charts on the range of f , μ_β and $\mu_{\beta'}$ be the Beltrami coefficients computed under $f_{\alpha\beta}$ and $f_{\alpha\beta'}$, respectively. We have

$$\begin{aligned} \mu_{\beta'}(z_\alpha) &= \frac{\partial f_{\alpha\beta'}}{\partial \bar{z}_\alpha} \Big/ \frac{\partial f_{\alpha\beta'}}{\partial z_\alpha} = \left(\frac{\partial w_{\beta'}}{\partial w_\beta} \frac{\partial f_{\alpha\beta}}{\partial \bar{z}_\alpha} + \frac{\partial w_{\beta'}}{\partial \bar{w}_\beta} \frac{\partial \bar{f}_{\alpha\beta}}{\partial \bar{z}_\alpha} \right) \Big/ \left(\frac{\partial w_{\beta'}}{\partial w_\beta} \frac{\partial f_{\alpha\beta}}{\partial z_\alpha} + \frac{\partial w_{\beta'}}{\partial \bar{w}_\beta} \frac{\partial \bar{f}_{\alpha\beta}}{\partial z_\alpha} \right) \\ &= \frac{\partial f_{\alpha\beta}}{\partial \bar{z}_\alpha} \Big/ \frac{\partial f_{\alpha\beta}}{\partial z_\alpha} = \mu_\beta(z_\alpha), \end{aligned} \tag{3}$$

since $w_{\beta'}$ is holomorphic and so $\frac{\partial w_{\beta'}}{\partial \bar{w}_\beta} = 0$.

Now we consider the properties of the composed mapping.

Definition 3.3 (*Composition of Quasiconformal Mappings*) Let $f : S_1 \rightarrow S_2$ be a QC mapping with Beltrami coefficient μ_f , $g : S_2 \rightarrow S_3$ be a QC mapping associated with Beltrami coefficient μ_g . The composed mapping $g \circ f : S_1 \rightarrow S_3$ is a QC mapping with Beltrami coefficient

$$\mu_{g \circ f} = \frac{\mu_f + (\mu_g \circ f)\tau}{1 + \bar{\mu}_f(\mu_g \circ f)\tau}, \quad \tau = \frac{\bar{f}_{\bar{z}}}{f_z}. \tag{4}$$

Lemma 3.4 (QC-Conformal Invariance) *Suppose $f : S_1 \rightarrow S_2$ is a QC mapping associated with the Beltrami differential μ_f , g is a conformal mapping of $f(S_1)$ ($\mu_g = 0$). Then $g \circ f : S_1 \rightarrow S_2$ is a QC mapping with Beltrami coefficient*

$$\mu_{g \circ f} = \mu_f.$$

The Beltrami differential is invariant to all conformal transformations of the target surface. This can be verified by Eq. (3).

Lemma 3.5 (Conformal-QC Variance) *Suppose $f : S_1 \rightarrow S_2$ is a conformal mapping ($\mu_f = 0$), $g : S_2 \rightarrow S_3$ is a QC mapping associated with the Beltrami differential μ_g . Then $g \circ f : S_1 \rightarrow S_3$ is a QC mapping with Beltrami coefficient*

$$\mu_{g \circ f} = (\mu_g \circ f)\tau, \quad \tau = \frac{\bar{f}_z}{f_z}.$$

This can be verified by Eq. (2).

Figures 4 and 5 demonstrate the intuitive meaning of the above two lemmas, by composing the conformal and QC mappings in different orders. Figure 4 explains Lemma 3.4. S_1 is a human face surface acquired from a 3D scanner. A QC mapping $f : S_1 \rightarrow S_2$ maps it to the planar unit disk S_2 . $g : S_2 \rightarrow S_3$ is a Möbius transformation of the disk, which is conformal. In order to visualize the Beltrami coefficients induced by the mappings, we use texture mapping method in modern graphics. In frame (e), we put a circle packing texture on S_2 , then the circle field on S_2 is pulled back onto S_1 by f . Since f is QC, the pullback circle field becomes an ellipse field. The eccentricity and orientation of the ellipses indicate the Beltrami coefficient μ_f . Similarly, we put a circle packing texture on S_3 and pull it back to S_1 by $g \circ f$. The Beltrami coefficient $\mu_{g \circ f}$ can be visualized in frame (f). Carefully examine (e) and (f), we can verify that at the same point on S_1 , such as the corner of eyes, the ellipse on (e) and that on (f) share the **same** eccentricity and **same** orientation, but have **different** sizes. This shows μ_f equals to $\mu_{g \circ f}$.

Similarly, Fig. 5 explains Lemma 3.5. S_1, S_2, S_3 are unit disks. $f : S_1 \rightarrow S_2$ is a Möbius transformation. $g : S_2 \rightarrow S_3$ is a QC-mapping, where $\mu_g(z) = 0.5z, z \in \mathbb{D}$. We put a circle packing texture on S_3 , and pull it back by g to obtain the ellipse field on S_2 , as shown in (e). Then μ_g is visualized by the ellipse field in (e). We put a circle packing texture on S_3 , and pull it back by $g \circ f$ to obtain the ellipse field on S_1 , as shown in (f). Carefully examine (e) and (f), we can see that for the same point p on S_1 and the corresponding point $f(p)$ on S_2 , e.g. the nose tip, eye corners, the ellipse at p in (e) and that of $f(p)$ in (f), have the **same** eccentricity, but **different** orientations and **different** sizes. This demonstrates $\mu_g(f(p))$ and $\mu_{g \circ f}(p)$ have the **same** norm, but **different** argument.

In this work, our goal is to compute numerically the QC mapping associated with a given Beltrami differential.

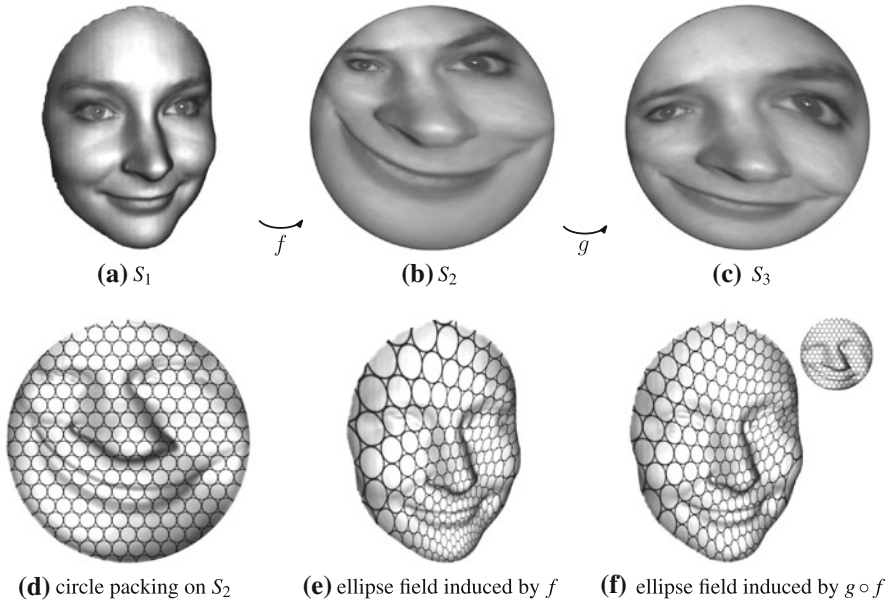


Fig. 4 Beltrami coefficients of the composed mappings. μ_f equals to $\mu_{g \circ f}$, where g is a conformal mapping

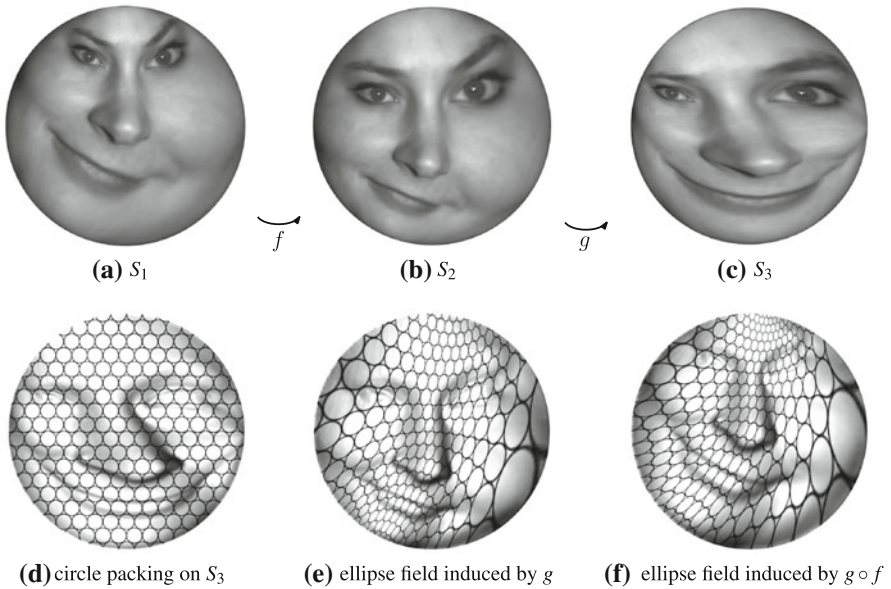


Fig. 5 Beltrami coefficients of the composed mappings. μ_g and $\mu_{g \circ f}$ differ by a rotation, where f is a conformal mapping

3.3 Uniformization theorem and Yamabe flow

Let S be a surface embedded in \mathbb{R}^3 with the induced Euclidean metric \mathbf{g} . We say another Riemannian metric $\bar{\mathbf{g}}$ is *conformal* to \mathbf{g} , if there is a scalar function $u : S \rightarrow \mathbb{R}$, such that $\bar{\mathbf{g}} = e^{2u}\mathbf{g}$. The Gaussian curvature K induced by $\bar{\mathbf{g}}$ is

$$\bar{K} = e^{-2u}(-\Delta_{\mathbf{g}}u + K),$$

where $\Delta_{\mathbf{g}}$ is the Laplace–Beltrami operator under the original metric \mathbf{g} . The above equation is called the *Yamabe equation*. By solving the Yamabe equation for u , one can design a conformal metric $e^{2u}\mathbf{g}$ by prescribing a curvature \bar{K} .

The Yamabe equation can be solved using the *Ricci flow* method [32]. The Ricci flow deforms the metric $\mathbf{g}(t)$ according to the Gaussian curvature $K(t)$ (induced by itself), where t is the time parameter

$$\frac{d\mathbf{g}(t)}{dt} = 2(\bar{K} - K(t))\mathbf{g}(t).$$

The *uniformization theorem* for surfaces says that any metric surface admits a conformal metric, which induces constant Gaussian curvature. The constant is one of $\{-1, 0, +1\}$, determined by the topology of the surface. Such a metric is called the *uniformization metric*. Ricci flow converges to the uniformization metric. Detailed proofs can be found in [14,31].

As the surface curvature flow methods, the smooth Yamabe flow and the smooth Ricci flow are equivalent. However, their numerically computational algorithm are different due to their different discretization solution [35,60].

3.4 Auxiliary metric for solving Beltrami equation

Here, we prove the main theorem of this paper, which allows us to define an auxiliary metric to solve the Beltrami equation on Riemann surfaces.

Theorem 3.6 (Auxiliary Metric Associated with A Beltrami Differential) *Suppose (S_1, \mathbf{g}_1) and (S_2, \mathbf{g}_2) are two metric surfaces, $f : S_1 \rightarrow S_2$ is a QC mapping associated with the Beltrami differential $\mu \frac{d\bar{z}}{dz}$. Let z and w be the local isothermal coordinates of S_1 and S_2 respectively, indeed $\mathbf{g}_1 = e^{2\lambda_1(z)} dz d\bar{z}$ and $\mathbf{g}_2 = e^{2\lambda_2(w)} dw d\bar{w}$. Define an auxiliary Riemannian metric on S_1 ,*

$$\tilde{\mathbf{g}}_1 = e^{2\lambda_1(z)} |dz + \mu d\bar{z}|^2. \tag{5}$$

The auxiliary metric $\tilde{\mathbf{g}}_1$ is well-defined and the mapping $f : (S_1, \tilde{\mathbf{g}}_1) \rightarrow (S_2, \mathbf{g}_2)$ is a conformal mapping.

Proof We first prove the auxiliary metric $\tilde{\mathbf{g}}_1$ is well-defined. Consider the region which is covered by two different charts z_α and z_β . Suppose the local representations of \mathbf{g}_1 under z_α and z_β are $e^{2\lambda_\alpha(z)} dz_\alpha d\bar{z}_\alpha$ and $e^{2\lambda_\beta(z)} dz_\beta d\bar{z}_\beta$, respectively.

Since $\frac{dz_\alpha}{d\bar{z}_\beta} = 0$, we have

$$dz_\alpha = \frac{dz_\alpha}{dz_\beta} dz_\beta + \frac{dz_\alpha}{d\bar{z}_\beta} d\bar{z}_\beta = \frac{dz_\alpha}{dz_\beta} dz_\beta, \text{ and}$$

$$e^{2\lambda_\alpha(z_\alpha)} dz_\alpha d\bar{z}_\alpha = e^{2\lambda_\alpha(z_\alpha)} |dz_\alpha|^2 = e^{2\lambda_\alpha(z_\alpha)} \left| \frac{dz_\alpha}{dz_\beta} \right|^2 |dz_\beta|^2 = e^{2\lambda_\beta(z_\beta)} dz_\beta d\bar{z}_\beta,$$

which gives $e^{2\lambda_\beta(z_\beta)} = e^{2\lambda_\alpha(z_\alpha)} \left| \frac{dz_\alpha}{dz_\beta} \right|^2$.

Thus, with Eq. (1),

$$\begin{aligned} e^{2\lambda_\alpha(z_\alpha)} |dz_\alpha + \mu_\alpha d\bar{z}_\alpha|^2 &= e^{2\lambda_\alpha(z_\alpha)} \left| \frac{dz_\alpha}{dz_\beta} dz_\beta + \mu_\alpha \frac{d\bar{z}_\alpha}{d\bar{z}_\beta} d\bar{z}_\beta \right|^2 \\ &= e^{2\lambda_\alpha(z_\alpha)} \left| \frac{dz_\alpha}{dz_\beta} \right|^2 \left| dz_\beta + \mu_\alpha \frac{d\bar{z}_\alpha}{d\bar{z}_\beta} / \frac{dz_\alpha}{dz_\beta} d\bar{z}_\beta \right|^2 \\ &= e^{2\lambda_\beta(z_\beta)} |dz_\beta + \mu_\beta d\bar{z}_\beta|^2. \end{aligned}$$

To see the mapping $f : (S_1, \tilde{\mathbf{g}}_1) \rightarrow (S_2, \mathbf{g}_2)$ is a conformal mapping, let $f^*\mathbf{g}_2$ denote the pullback metric,

$$f^*\mathbf{g}_2 = e^{2\lambda_2(f(z))} |df(z)|^2.$$

Under the pullback metric, the mapping $f : (S_1, f^*\mathbf{g}_2) \rightarrow (S_2, \mathbf{g}_2)$ is isometric,

$$\begin{aligned} df(z) &= \frac{\partial f(z)}{\partial z} dz + \frac{\partial f(z)}{\partial \bar{z}} d\bar{z} \\ &= \frac{\partial f(z)}{\partial z} (dz + \mu d\bar{z}). \end{aligned}$$

Therefore,

$$f^*\mathbf{g}_2 = e^{2\lambda_2(f(z))} \left| \frac{\partial f(z)}{\partial z} \right|^2 |dz + \mu d\bar{z}|^2.$$

According to the definition of $\tilde{\mathbf{g}}_1$ in Eq. (5), $f^*\mathbf{g}_2 = e^{2\lambda_2(f(z)) - 2\lambda_1(z)} \left| \frac{\partial f(z)}{\partial z} \right|^2 \tilde{\mathbf{g}}_1$. $f^*\mathbf{g}_2$ is conformal to $\tilde{\mathbf{g}}_1$. Because $f : (S_1, f^*\mathbf{g}_2) \rightarrow (S_2, \mathbf{g}_2)$ is isometric, therefore $f : (S_1, \tilde{\mathbf{g}}_1) \rightarrow (S_2, \mathbf{g}_2)$ is conformal.

This theorem tells us in order to solve the Beltrami equation on Riemann surfaces, we simply need to define a new auxiliary metric associated with the prescribed Beltrami differential. We can then solve the Beltrami equation by computing a conformal mapping associated with the newly defined metric. In other words, the QC mapping is equivalent to a conformal mapping under a suitable auxiliary metric. This observation is important for us to develop the numerical algorithm to compute QC mappings (See Sect. 5).

4 Discrete quasiconformal mapping using auxiliary metric

In Sect. 3, we briefly discuss the theory of QC geometry and describe the auxiliary metric on smooth Riemann surfaces. In practice, most surfaces are approximated by simplicial complexes, namely triangular meshes. It is therefore necessary to have a discrete analog of QC geometry on discrete meshes. In this section, we will formulate the definitions of *discrete quasiconformal mappings* and their associated *discrete Beltrami differentials*.

Suppose M is triangular mesh, V, E, F are vertex, edge and face set respectively. We denote v_i as the i th vertex; $[v_i, v_j]$ as the oriented edge from v_i to v_j ; $[v_i, v_j, v_k]$ as the face, where the vertices are sorted counter-clockwisely. On triangular meshes, we can derive a discrete version of Yamabe flow, called the *discrete Yamabe flow*, which is analogous to the curvature flow on smooth surfaces. In this section, we describe in detail the discrete Euclidean and hyperbolic Yamabe flow that converge to the Euclidean and hyperbolic uniformization metric respectively.

On the discrete mesh, we can define the discrete metric, which is similar to the Riemannian metric. Basically, the discrete metric gives the length of each edge.

Definition 4.1 (*Discrete Metric*) A discrete metric on a mesh M is a function $l : E \rightarrow \mathbb{R}^+$, such that on each triangle $[v_i, v_j, v_k]$, the triangle inequality holds,

$$l_{jk} + l_{ki} > l_{ij},$$

where $l_{jk} = l[v_j, v_k]$, $l_{ki} = l[v_k, v_i]$ and $l_{ij} = l[v_i, v_j]$.

Discrete metric represents a configuration of edge lengths. As shown in Fig. 6(a), different background geometries can be assigned to a mesh.

Definition 4.2 (*Background Geometry*) Suppose M is a mesh with a discrete metric. If all faces are Euclidean, or Hyperbolic triangles, then the mesh is with Euclidean, or Hyperbolic background geometry, denoted as \mathbb{E}^2 , or \mathbb{H}^2 .

Discrete metric determines the corner angles on each face by the cosine law,

$$\theta_i = \begin{cases} \cos^{-1} \frac{l_{ki}^2 + l_{ij}^2 - l_{jk}^2}{2l_{ki}l_{ij}} & \mathbb{E}^2 \\ \cos^{-1} \frac{\cosh l_{ki} \cosh l_{ij} - \cosh l_{jk}}{2 \sinh l_{ki} \sinh l_{ij}} & \mathbb{H}^2 \end{cases}.$$

Definition 4.3 (*Discrete Conformal Deformation*) Let M be a triangulation mesh. Suppose l and L are two different discrete metrics on M . L is a *discrete conformal deformation* of l if there exists a function $u : V \rightarrow \mathbb{R}$, called *discrete conformal factor*, such that for all edges $[v_i, v_j] \in E$ on M :

$$L_{ij} = L[v_i, v_j] = \begin{cases} e^{u(v_i)} l_{ij} e^{u(v_j)} & \mathbb{E}^2 \\ 2 \sinh^{-1} e^{u(v_i)} \sinh(\frac{l_{ij}}{2}) e^{u(v_j)} & \mathbb{H}^2 \end{cases}.$$

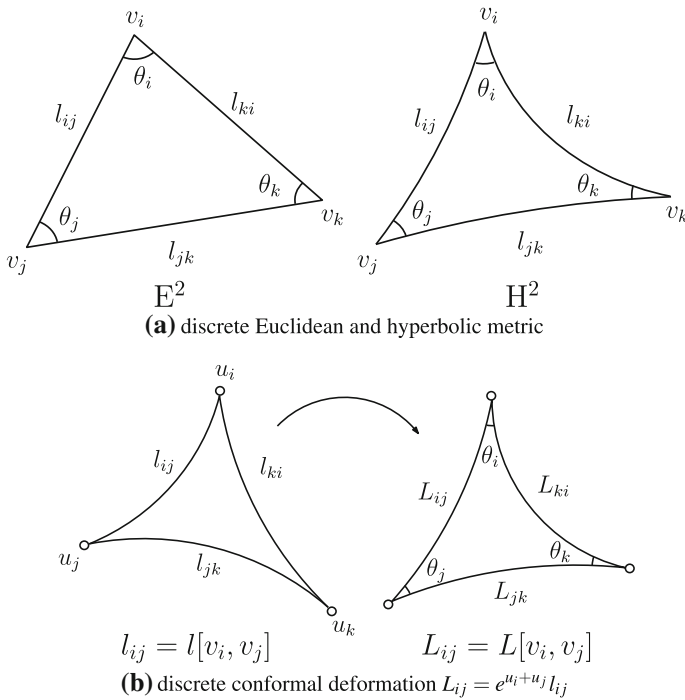


Fig. 6 Discrete metric and conformal deformation in Euclidean and hyperbolic cases: **a** the Euclidean and hyperbolic triangles and **b** the discrete conformal deformation by the discrete Yamabe flow. **a** discrete Euclidean and hyperbolic metric. **b** discrete conformal deformation $L_{ij} = e^{u_i + u_j} l_{ij}$

See Fig. 6(b). Note that the definition of discrete hyperbolic conformality was due to Springborn et al. [8].

Definition 4.4 (*Discrete Local Isothermal Chart*) Let M be a triangular mesh. A mesh M_α is called a *submesh* of M if every vertices, edges and faces of M_α belong to M . A *discrete local isothermal chart* $(M_\alpha, \phi_\alpha) : M_\alpha \rightarrow \mathbb{C}$ is a discrete conformal mapping from M_α to a mesh $\phi_\alpha(M_\alpha)$ embedded in \mathbb{C} .

Since the triangular meshes are considered as the discrete approximations of smooth surfaces, we can assume that the triangular meshes are covered by a collection of discrete local charts.

Definition 4.5 (*Discrete Beltrami Differential*) A *discrete Beltrami differential* $\{\mu_\alpha\}$ is an assignment to each discrete local isothermal chart (M_α, ϕ_α) on M_α of an L_∞ complex-valued function μ_α defined on every vertices of $\phi_\alpha(M_\alpha)$ with $|\mu_\alpha| < 1$, such that:

$$\frac{\mu_\alpha(v_i) + \mu_\alpha(v_j)}{2} \frac{\overline{z_\alpha(v_j) - z_\alpha(v_i)}}{z_\alpha(v_j) - z_\alpha(v_i)} = \frac{\mu_\beta(v_i) + \mu_\beta(v_j)}{2} \frac{\overline{z_\beta(v_j) - z_\beta(v_i)}}{z_\beta(v_j) - z_\beta(v_i)}, \quad (6)$$

where $[v_i, v_j]$ is any edge in the domain which is also covered by another chart (M_β, ϕ_β) .

By letting $\mu_{ij}^\alpha = \frac{\mu^\alpha(v_i) + \mu^\alpha(v_j)}{2}$, $\mu_{ij}^\beta = \frac{\mu^\beta(v_i) + \mu^\beta(v_j)}{2}$, $dz_{ij}^\alpha = z^\alpha(v_j) - z^\alpha(v_i)$ and $dz_{ij}^\beta = z^\beta(v_j) - z^\beta(v_i)$, Eq. (6) can be simplified as

$$\mu_{ij}^\alpha \frac{d\bar{z}_{ij}^\alpha}{dz_{ij}^\alpha} = \mu_{ij}^\beta \frac{d\bar{z}_{ij}^\beta}{dz_{ij}^\beta},$$

which is the discrete analog of Eq. (1).

Definition 4.6 (*Discrete Quasiconformal Mapping between Triangular Meshes*) Let $\{\mu_\alpha\}$ be a given discrete Beltrami differential. A mapping $f : (M_1, l) \rightarrow (M_2, L)$ between meshes M_1 and M_2 is a *discrete quasiconformal mapping*, if with respect to a new metric \tilde{l} on M_1 , the mapping $f : (M_1, \tilde{l}) \rightarrow (M_2, L)$ is discrete conformal, where

$$\tilde{l}_{ij} := l_{ij} \frac{|dz_{ij} + \mu_{ij} d\bar{z}_{ij}|}{|dz_{ij}|}, \quad \left(dz_{ij} = z(v_j) - z(v_i), \mu_{ij} = \frac{\mu_i + \mu_j}{2} \right), \quad (7)$$

for any local isothermal coordinates z of M_1 . \tilde{l} is called the *discrete auxiliary metric* associated with $\{\mu_\alpha\}$.

Note that the definition is well-defined. Suppose an edge $[v_i, v_j]$ is covered by both charts z_α and z_β , we have

$$\begin{aligned} l_{ij} \frac{|dz_{ij}^\alpha + \mu_{ij}^\alpha d\bar{z}_{ij}^\alpha|}{|dz_{ij}^\alpha|} &= l_{ij} \left| 1 + \mu_{ij}^\alpha \frac{d\bar{z}_{ij}^\alpha}{dz_{ij}^\alpha} \right| = l_{ij} \left| 1 + \mu_{ij}^\beta \frac{d\bar{z}_{ij}^\beta}{dz_{ij}^\beta} \right| \\ &= l_{ij} \frac{|dz_{ij}^\beta + \mu_{ij}^\beta d\bar{z}_{ij}^\beta|}{|dz_{ij}^\beta|}. \end{aligned}$$

The following analogous theorem of Theorem 3.6 is observed immediately from the above definitions of discrete QC mappings and discrete auxiliary metric.

Theorem 4.7 (*Discrete Auxiliary Metric Associated with a Beltrami Differential*) Suppose (M_1, l) and (M_2, L) are two metric triangular meshes, $f : M_1 \rightarrow M_2$ is a QC mapping, its Beltrami differential is $\{\mu_\alpha\}$. Under the auxiliary metric \tilde{l} associated with $\{\mu_\alpha\}$, the mapping $f : (M_1, \tilde{l}) \rightarrow (M_2, L)$ is discrete conformal.

Theorem 4.7 will be used for the computation of discrete QC mappings in Sect. 5.

5 Algorithm of discrete quasiconformal mapping

In this section, we describe in detail the numerical algorithm to compute the discrete QC mapping associated with a given Beltrami differential. Based on Theorem 4.7, the algorithm consists of two main steps: (1) Compute the discrete auxiliary metric

associated with the prescribed Beltrami differential; (2) Under the discrete auxiliary metric, compute the conformal parameterization using the discrete Yamabe flow method. Here, the algorithm to compute discrete QC mapping is called the *discrete Quasi-Yamabe flow*. Note that in this work, our QC mapping algorithm is based on the discrete Yamabe flow method. In general, our algorithm can be implemented with any conformal mapping methods.

5.1 Computation of auxiliary metric

The first step of our algorithm is to compute the auxiliary metric associated with a given Beltrami differential. The formula for computing the auxiliary metric is given in Eq. (7). The detailed computational algorithm can be summarized as follows:

Algorithm : Auxiliary Metric for Both \mathbb{E}^2 and \mathbb{H}^2 Background Geometry

Input : Triangular mesh $M = (V, E, F)$ with conformal parameterization $z : V \rightarrow \mathbb{C}$, and
 discrete Beltrami differential $\mu : V \rightarrow \mathbb{C}$ defined on the conformal structure.

Output : Discrete auxiliary metric \tilde{l}_{ij} for all edges $[v_i, v_j] \in E$.

For all Edge $[v_i, v_j] \in E$ **do**

1. Compute the edge length l_{ij} using the induced Euclidean metric;
2. Compute the derivative of conformal coordinates on $[v_i, v_j]$, $dz_{ij} \leftarrow z(v_j) - z(v_i)$;
3. Compute the Beltrami coefficient on $[v_i, v_j]$, $\mu_{ij} \leftarrow \frac{1}{2}(\mu(v_i) + \mu(v_j))$;
4. Compute the scalar of metric $\lambda_{ij} \leftarrow \frac{|dz_{ij} + \mu_{ij} dz_{ij}|}{|dz_{ij}|}$;
5. Compute the new auxiliary metric $\tilde{l}_{ij} \leftarrow \lambda_{ij} l_{ij}$.

End for

The computing procedure is unified for any Riemann surface. It is formulated as a scalar function for the original Euclidean metric from the given Beltrami differential μ and conformal chart z .

5.2 Conformal parameterization under auxiliary metric

After the discrete auxiliary metric is computed, we can then compute the discrete QC mapping simply by computing the discrete conformal mapping under the new metric. In general, we can apply any existing conformal mapping algorithms to compute the conformal mapping under the new auxiliary metric. Here, we will use the discrete Yamabe flow method to compute the conformal mapping. The discrete Yamabe flow iteratively and conformally deforms the metric on the source surface to a uniformization metric, which induces constant Gaussian curvature.

On a triangular mesh M , the discrete Gaussian curvature is defined as angle deficient. Suppose $[v_i, v_j, v_k]$ is a face in M , θ_i^{jk} represents the corner angle at v_i on the face. The discrete Gaussian curvature of v_i is defined as

$$K_i = \begin{cases} 2\pi - \sum_{jk} \theta_i^{jk} & v_i \notin \partial M \\ \pi - \sum_{jk} \theta_i^{jk} & v_i \in \partial M \end{cases}.$$

Now, suppose the discrete conformal deformation under the discrete Yamabe flow is given by the discrete conformal factor $u : V \rightarrow \mathbb{R}$ (See Definition 4.5). Let \bar{K}_i denote the target curvature at v_i . The discrete Yamabe flow has the following formula:

$$\frac{du_i}{dt} = \bar{K}_i - K_i.$$

The discrete Yamabe flow is the negative gradient flow of the Yamabe energy. Let $\mathbf{u} = (u_1, u_2, \dots, u_n)$ and $\mathbf{u}_0 = (0, 0, \dots, 0)$. The discrete Yamabe energy has the form:

$$E(\mathbf{u}) = \int_{\mathbf{u}_0}^{\mathbf{u}} \sum_{i=1}^n (\bar{K}_i - K_i) du_i.$$

The Hessian matrix $H = (h_{ij})$ of E can be computed explicitly. Let $[v_i, v_j]$ be an edge, connecting two faces $[v_i, v_j, v_k]$ and $[v_j, v_i, v_l]$, then the Hessian matrix satisfies

$$h_{ij} = \frac{\partial \theta_i^{jk}}{\partial u_j} + \frac{\partial \theta_i^{lj}}{\partial u_j}, \quad i \neq j \quad \text{and} \quad h_{ii} = \sum_{j,k} \frac{\partial \theta_i^{jk}}{\partial u_i},$$

where the summation goes through all faces surrounding $v_i, [v_i, v_j, v_k]$. Here,

$$\frac{\partial \theta_i}{\partial u_i} = \begin{cases} -\cot \theta_j - \cot \theta_k & \mathbb{E}^2 \\ -\frac{2c_i c_j c_k - c_j^2 - c_k^2 + c_i c_j + c_i c_k - c_j - c_k}{A(c_j+1)(c_k+1)} & \mathbb{H}^2 \end{cases} \quad \text{and} \quad \frac{\partial \theta_i}{\partial u_j} = \begin{cases} \cot \theta_k & \mathbb{E}^2 \\ \frac{c_i + c_j - c_k - 1}{A(c_k+1)} & \mathbb{H}^2 \end{cases}, \tag{8}$$

where in \mathbb{H}^2 case, $c_k = \cosh(L_{ij})$ and $A = \sin(\theta_k) \sinh(L_{jk}) \sinh(L_{ki})$.

Using the Newton’s method, the discrete Yamabe flow now reads as follows

$$u^{n+1} = u^n + \delta^n,$$

where $H\delta^n = \bar{K} - K^n$. Note that the Hessian $H = (h_{ij})$ is sparse. The entry h_{ij} is non-zero if and only if v_i and v_j are adjacent to each other. In this work, we use the conjugate gradient method to solve the linear system for δ^n . After computing the discrete metric of the mesh, we can embed the mesh onto \mathbb{E}^2 or \mathbb{H}^2 . Basically, we can isometrically flatten triangle by triangle using the Euclidean or hyperbolic cosine law. For more details about the discrete Yamabe flow, we refer readers to [60].

The discrete conformal complex structure for a triangular mesh is computed by the discrete Yamabe flow. The quasiconformality of the desired discrete QC mapping is determined by the given discrete Beltrami differential μ , with respect to each vertex. The proposed auxiliary metric, inducing the quasiconformality, is obtained from the Beltrami differential and the original conformal structure. The resulting conformal mapping of the discrete Yamabe flow under the new auxiliary metric is a discrete

QC mapping of the original mesh, associated with the predefined discrete Beltrami differential. The numerical convergency proof is described in Sect. 6. The proposed method here to compute QC mapping under the new auxiliary metric is called *discrete Quasi-Yamabe flow* method.

6 Convergency of discrete Quasi-Yamabe flow

We now study the numerical convergency of our proposed discrete Quasi-Yamabe flow method. The convergence of metric under the discrete Yamabe flow is discussed in [16].

Firstly, the convexity of the Yamabe energy can be obtained by carefully examining the positive definiteness of the Hessian matrix $H = (h_{ij})$. The computational details are shown in Eq. (8).

Theorem 6.1 *The discrete Yamabe energy is locally convex on the space of $\sum_i u_i = 0$ in the Euclidean case. The discrete Yamabe energy is locally convex in the hyperbolic case.*

Proof The local convexity of the Euclidean Yamabe energy is due to the fact that the Hessian matrix $H = (h_{ij})$ of $E(\mathbf{u})$ is semi-positive definite. Clearly, the summation of each row is zero and only the diagonal elements are positive. Furthermore, since the matrix is positive definite on the linear space $\sum_i u_i = 0$, it follows that H is locally strictly convex on the planes. For details, please see [46].

We now prove the local convexity of the hyperbolic Yamabe energy. This fact was also known to Springborn et al. [8]. We prove the Hessian matrix of the hyperbolic Yamabe energy is positive definite. Let l_1, l_2, l_3 be the lengths of a hyperbolic triangle. Make conformal change to produce a new hyperbolic triangle of lengths L_1, L_2, L_3 , so that $\sinh(L_i/2) = \sinh(l_i/2)e^{u_j+u_k}$, $\{i, j, k\} = \{1, 2, 3\}$. Let θ_i represent the corner angle at the vertex v_i , $H = [\frac{\partial \theta_i}{\partial u_j}]$ be the matrix.

Fact 1 : $\det(H) \neq 0$ for all u 's. Indeed, the mapping from $(u_1, u_2, u_3) \rightarrow (\theta_1, \theta_2, \theta_3)$ is a diffeomorphism.

Fact 2 : For any (l_1, l_2, l_3) in the set of all $\mathbf{u} = (u_1, u_2, u_3)$ such that $L_i/2 = 2 \sinh^{-1}(\sinh(l_i/2)e^{u_j+u_k})$ satisfies triangular inequalities: $L_1 + L_2 > L_3$, $L_1 + L_3 > L_2$ and $L_2 + L_3 > L_1$, which form a connected set Ω in \mathbb{R}^3 .

Fact 3 : Since Ω is connected and H is symmetric in Ω so that $\det(H) \neq 0$, the signature of H is a constant.

Fact 4 : Choose those u_1, u_2, u_3 so that $L_1 = L_2 = L_3$, we see easily by computation that the Hessian H is positive definite.

Thus, H is positive definite over all Ω .

Now to prove **Fact 2** : Introduce a new variable $t_i = e^{u_j+u_k}$. The mapping $\mathbf{u} \mapsto \mathbf{t}$ is a diffeomorphism. Thus, it suffices to prove that the set

$$\Omega^1 = \{(t_1, t_2, t_3) \in \mathbb{R}_{>0}^3 \mid L_i = 2 \sinh^{-1}(t_i \sinh(\frac{a_i}{2}))$$

satisfy the triangle inequality

is connected. Fix t_2, t_3 , we will show that the set of all \mathbf{t} such that

$$\begin{aligned}
 & \left| \sinh^{-1} \left(t_2 \sinh \left(\frac{a_2}{2} \right) \right) - \sinh^{-1} \left(t_3 \sinh \left(\frac{a_3}{2} \right) \right) \right| < \sinh^{-1} \left(t_2 \sinh \left(\frac{a_2}{2} \right) \right) \\
 & + \sinh^{-1} \left(t_3 \sinh \left(\frac{a_3}{2} \right) \right)
 \end{aligned}$$

is connected. This is obvious since $f(t) = \sinh^{-1}(t)$ is a strictly increasing function in t .

The discrete Yamabe energy can be optimized using Newton’s method directly. Given the mesh M , a conformal factor vector \mathbf{u} is *admissible*, if the deformed metric satisfies the triangle inequality on each face. The space of all admissible conformal factors is not convex in either Euclidean or Hyperbolic case. In practice, the step length in Newton’s method needs to be adjusted. Also, the triangle inequality is a requirement for a legitimate triangulation mesh. During the discrete Yamabe flow, the triangle inequality might fail to hold (which rarely occurs in practice, except for very irregular meshes). If such case occurs, one can do surgery changes by edge swapping to remove the singularity. After finitely many such surgery operations on the triangulation mesh, there will be no singularity developed in the normalized discrete Yamabe flow. We can then prove the the discrete Quasi-Yamabe flow starting from the auxiliary metric converges exponentially fast to the constant curvature metric.

Theorem 6.2 *If no singularity develops in the discrete Quasi-Yamabe flow after finitely many of surgery operations, the discrete auxiliary metric converges exponentially fast to a discrete uniformization metric with constant curvature as time approaches infinity. In other words,*

$$|K_i(t) - \bar{K}_i| \leq c_1 e^{-c_2 t}$$

for some constants c_1 and c_2 , and $K_i(t)$ is the discrete curvature at vertex v_i at time t .

Proof The solution $\mathbf{u}(t) = (u_1(t), \dots, u_N(t))$ of the discrete Yamabe flow exists for all time so that there are no singularities forming at time equal to infinity. This means that $u_i(t)$ ’s are in some compact interval in $\mathbb{R}_{>0}$ and also all inner angles $\theta_i^{ij}(t)$ are in some compact interval inside the interval $(0, \pi)$. The matrix $(h_{ij}) = (\frac{\partial \theta_i}{\partial u_j})$ has properties that the sum of entries in every row is zero and the diagonal entries are negative. (h_{ij}) is symmetric and semi-negative definite. This implies that there is a positive constant λ so that the eigenvalues of (h_{ij}) considered as a bilinear form restricted to the subspace $\{w \in \mathbb{R}^N | w_1 + \dots + w_N = 0\}$ is always bounded by $-\lambda$ for all time $t \in [0, \infty)$, i.e.,

$$\sum_{i,j} h_{ij} w_i w_j \leq -\lambda \sum_i w_i^2, \quad \text{when } \sum_{i=1}^N w_i = 0.$$

Note that

$$\frac{dK_i(t)}{dt} = \frac{d}{dt} \left(2\pi - \sum_{j,k} \theta_i^{jk} \right) = - \sum_{j,k} \frac{d\theta_i^{jk}}{dt} = - \sum_j \frac{\partial \theta_i}{\partial u_j} \frac{du_j}{dt} = \sum_j \frac{\partial \theta_i}{\partial u_j} (K_j - \bar{K}_j).$$

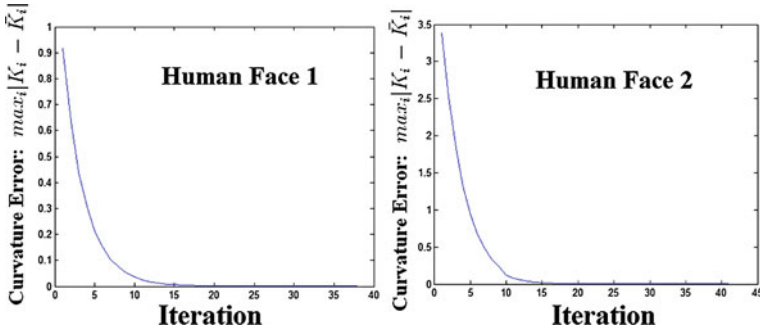


Fig. 7 The exponential convergence of the discrete Yamabe flow method. The curvature approximate error at each iteration is plotted for two human faces respectively

Now, consider $G(t) = \sum_{i=1}^N (K_i(t) - \bar{K}_i)^2$. Its derivative can be calculated as

$$G'(t) = 2 \sum_{i,j} h_{ij} (K_i - \bar{K}_i)(K_j - \bar{K}_j).$$

We have, $G'(t) \leq -\lambda G(t)$. Thus, $G(t) \leq C e^{-\lambda t}$, and so

$$|K_i(t) - \bar{K}_i| \leq c_1 e^{-c_2 t}.$$

Figure 7 shows the exponential convergence of the discrete Yamabe flow method. The curvature approximate error $\max_i |K_i - \bar{K}_i|$ at each iteration of two different real human faces is plotted on the left and right respectively.

Theorem 6.3 *Let $f : (S_1, \mathbf{g}_1) \rightarrow (S_2, \mathbf{g}_2)$ be a QC mapping with Beltrami differential $\mu \frac{\bar{d}z}{dz}$, with S_1 and S_2 are both of disk topology. Suppose \tilde{f}_h is a discrete QC mapping associated with $\{\mu_\alpha\}$ given by $\mu \frac{\bar{d}z}{dz}$ on a triangulation mesh with regular tessellation and mesh grid size h , which approximates f . Then $\tilde{f}_h \rightarrow f$ as $h \rightarrow 0$.*

Proof The proof that a discrete conformal mapping converges to a continuous conformal mapping under regular triangulation mesh was given by Bucking [11]. Therefore, the discrete mapping \tilde{f}_h converges to the conformal mapping $f_{AM} : (S_1, \tilde{\mathbf{g}}_1) \rightarrow (S_2, \mathbf{g}_2)$ under the auxiliary metric $\tilde{\mathbf{g}}_1$ associated with $\mu \frac{\bar{d}z}{dz}$ on S_1 . By Theorem 3.6, the conformal mapping $f_{AM} : (S_1, \tilde{\mathbf{g}}_1) \rightarrow (S_2, \mathbf{g}_2)$ is in fact a QC mapping $f : (S_1, \mathbf{g}_1) \rightarrow (S_2, \mathbf{g}_2)$ with Beltrami differential $\mu \frac{\bar{d}z}{dz}$ under the original metric \mathbf{g}_1 on S_1 . Thus, $\tilde{f}_h \rightarrow f$ as $h \rightarrow 0$.

7 Experimental results

We implement our algorithm using generic C++ on Windows platform. The linear systems are solved using the conjugate gradient method. The experiments are carried

Table 2 Computational time

Figure	1	9	10	12	13	14	15
Vertices#	20184	20184	25220	15306	13515	10000	2057
Faces#	39984	39984	49982	29990	26304	20000	4118
Time(s)	101	99	131	87	108	25	31

out on a laptop with 2.0GHZ CPU, 3.00G RAM. The human face surfaces are captured using phase shifting structured light method. Computational time is reported in Table 2.

7.1 Quasiconformal mappings for topological disks

Figure 1 shows the QC mapping for a real human face surface, which is a topological disk and is acquired from a 3D scanner. The Yamabe flow conformally maps the surface onto a planar unit disk \mathbb{D} , as shown in frame (c). We chose the Beltrami coefficients as $\mu(z) = 0.5z$, $z \in \mathbb{D}$. The QC mapping using the auxiliary metric based on Quasi-Yamabe flow is given in frame (f). We also demonstrate the concept of the chain rule of conformal and QC mappings on the topological disk surface, as shown in Figs. 4 and 5. The Möbius transformation is given by

$$z \rightarrow \frac{z - z_0}{1 - \bar{z}_0 z},$$

where z_0 is the point which will be moved the origin of the unite disk. The Beltrami coefficients are also chosen to be $\mu(z) = 0.5z$, $z \in \mathbb{D}$. Figure 8 illustrates the mesh deformation during the conformal and QC mappings on the topological disk, which includes 39,984 triangular faces.

7.2 Quasiconformal mappings for topological quadrilaterals

Figure 9 shows the experimental results for QC mappings of the human face surface, which is a topological quadrilateral with four fixed corners. The original face is shown in the top left corner. Four corner vertices are selected on the boundary, shown as p_0, p_1, p_2, p_3 . We set the target curvature to be $\frac{\pi}{2}$ for those four corner vertices, and zero for all vertices everywhere else (including boundary and interior vertices). The Yamabe flow conformally maps the surface onto a planar rectangle, as shown in frames (a) and (b). The corner vertices are mapped to the rectangle corners. We set the left lower corner to be the origin, the edges to be parallel to the axes, the width to be 1. Then the height h gives us the conformal module of the original face surface with four fixed corners. This provides us the conformal parameter z of the surface.

In frames (c–e), we set different Beltrami coefficients. The image of the QC mapping is shown on the left, the circle packing texture mapping is shown on the right. The Beltrami coefficient is set to be $\mu = \frac{z - z_0}{2\sqrt{1 + h^2}}$, with different values of z_0 for different

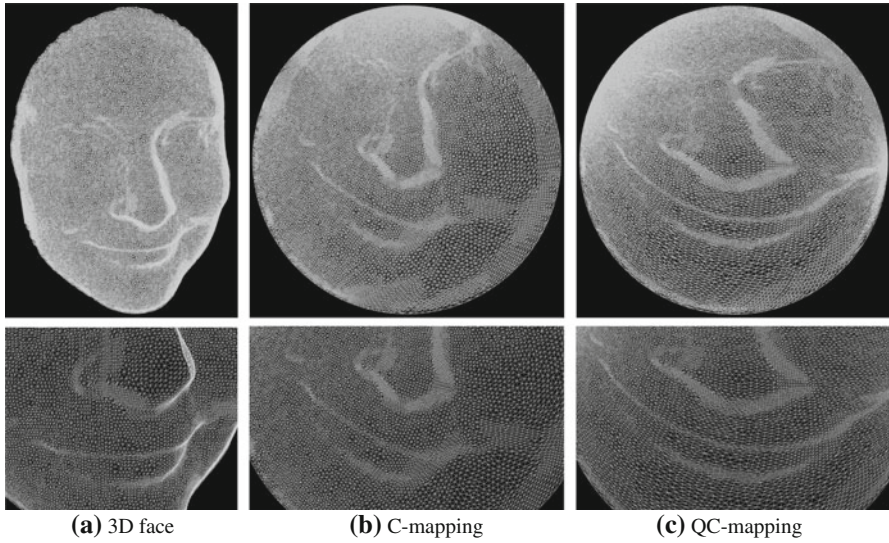


Fig. 8 Meshing deformation during conformal and quasiconformal mappings for a topological disk. The conformal parameter domain is a planar unit disk. The Beltrami coefficients for QC-mapping are $\mu(z) = 0.5z, z \in \mathbb{D}$. The second row shows the zoomed-in triangles

cases. It is obvious that, the conformal module of the surface changes with different Beltrami coefficients.

7.3 Composition of quasiconformal mappings

In the following experiment, we test the accuracy of our algorithm by computing the composed QC mappings using different approaches, and comparing their difference. If our method is accurate, the difference between the results obtained from the two approaches should be small.

Let $f : S \rightarrow D_1$ be a QC mapping with Beltrami coefficient $\mu_f, g : D_1 \rightarrow D_2$ be a conformal mapping with Beltrami coefficient μ_g . Then the composed mapping $g \circ f : S \rightarrow D_2$ should have the Beltrami coefficient in Eq. (4). As shown in Fig. 10, in our experiment, the original surface is a human face surface with four corner points (a topological quadrilateral), then we compute its conformal parameter domain, as shown in (a) and (b). Then we set the Beltrami coefficient μ_f to be $0.15 + i0.15$, and use our method to compute a QC mapping $f : S \rightarrow D_1$. The mapping result of f is shown in (c). We set $\mu_g = 0.15 + i0.15$, and compute the QC mapping $g : D_1 \rightarrow D_2$, as shown in (d).

We use the formula in Eq. (4) to compute the Beltrami coefficient for the composed mapping $\mu_{g \circ f} = 0.34 + i0.12$. We then solve the Beltrami equation $h_{\bar{z}} = \mu_{g \circ f} h_z$ to get a QC mapping $h : S \rightarrow D_2$, as shown in (e). In theory, h should coincide with $g \circ f$. Our experimental result shows that h is consistent with $g \circ f$. By comparing the results in (d) and (e), we can see the results of $g \circ f$ and h are almost identical. We further measure the deviation between them numerically, using the following formula,

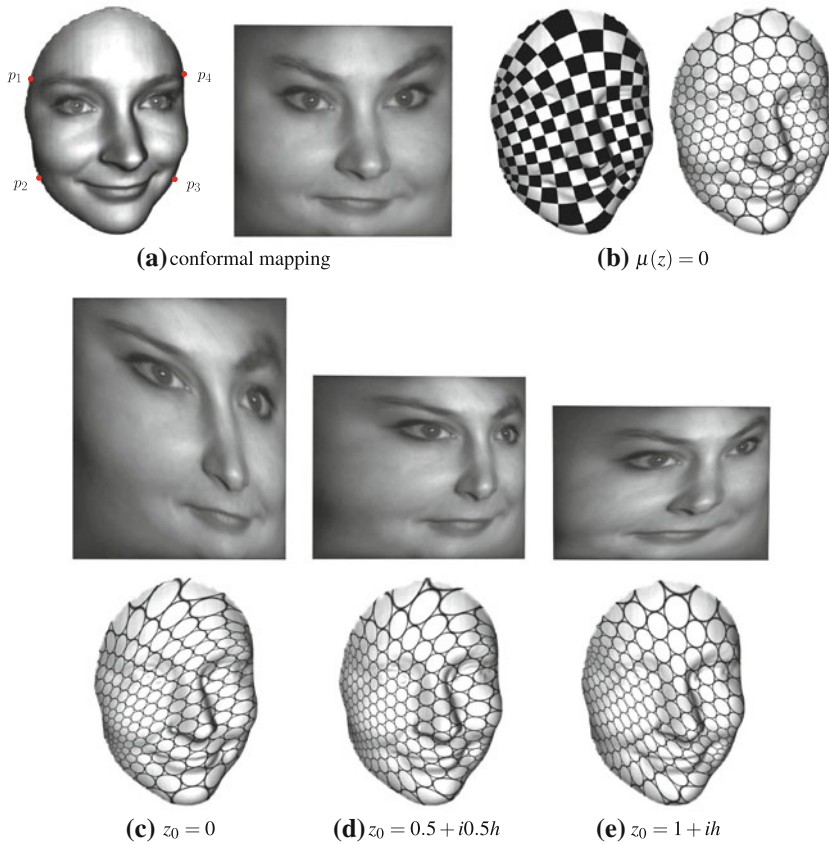


Fig. 9 Conformal and quasiconformal mappings for a topological quadrilateral. The conformal parameter domain is a rectangle with unit width and h height. For all other rows $\mu = \frac{z-z_0}{2\sqrt{1+h^2}}$ with different z_0 's

$$d(f, g) = \frac{1}{diag(S)A} \int_S |f(p) - g(p)| dp,$$

where A is the area of S , $diag(S)$ is the diagonal of the bounding box of S . The distance is the L^1 norm between f and g , normalized by the diagonal of surface. In our experiment, the distance is 0.000044, which is very small. This shows that our QC mapping method is accurate. Figure 11 shows the histogram of the real part, imaginary part and argument of μ_f, μ_g and $\mu_{f \circ g}$. (a), (b) and (c) shows the histograms of the real part, imaginary part and argument of the Beltrami coefficient μ_f of f computed by our method. The histograms show that $\mathbf{Real}(\mu_f) = 0.15$, $\mathbf{Imag}(\mu_f) = 0.15$ and $\mathbf{arg}(\mu_f) = 0.7854$ on almost all vertices, which agree with the exact solution, $\mu_g = 0.15 + i0.15$. (d), (e) and (f) shows the histograms of the Beltrami coefficient μ_g of g . (g), (h) and (i) shows the histogram of the real part, imaginary part and argument of the Beltrami coefficient $\mu_{f \circ g}$ of the composition mapping $g \circ f$. The histograms

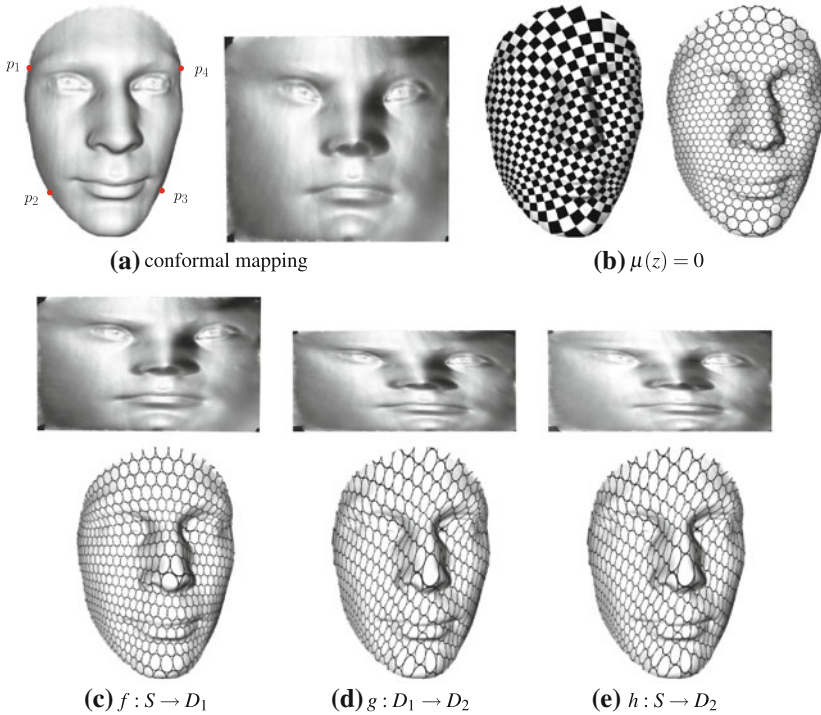


Fig. 10 Composition of quasiconformal mappings for a topological quadrilateral: $\mu_f = 0.15 + 0.15i$, $\mu_g = 0.15 + 0.15i$, and $h = g \circ f$, $\mu_h = \mu_{g \circ f} = 0.35 + 0.12i$ computed by Eq. (4)

show that $\mathbf{Real}(\mu_{g \circ f}) = 0.35$, $\mathbf{Imag}(\mu_{g \circ f}) = 0.12$ and $\mathbf{arg}(\mu_{g \circ f}) = 0.34$ on almost all vertices, which agree with the exact solution.

7.4 Quasiconformal mappings for topological annuli

Figures 12 and 13 show the QC mappings for genus zero surfaces with multiply holes. In Fig. 12, the human face surface is sliced open along the lip of the mouth which results in a doubly-connected open surface. Again, we set different Beltrami coefficients and compute the associated discrete auxiliary metrics. Using the discrete Yamabe flow, we conformally map the surface onto the annulus with respect to different auxiliary metrics. The target curvature is set to be zero in the interior and constant along the boundaries. The radius of the inner circles are different with different Beltrami coefficients, indicating a change in the conformal module. Figure 13 shows the similar results for the genus zero human face surface with three slices (topological disk with 3 holes).

7.5 Quasiconformal mappings for genus one surfaces

We test our algorithm for genus one closed surface as shown in Fig. 14. We first set μ to be zero, and compute a conformal flat metric using the curvature flow. Then

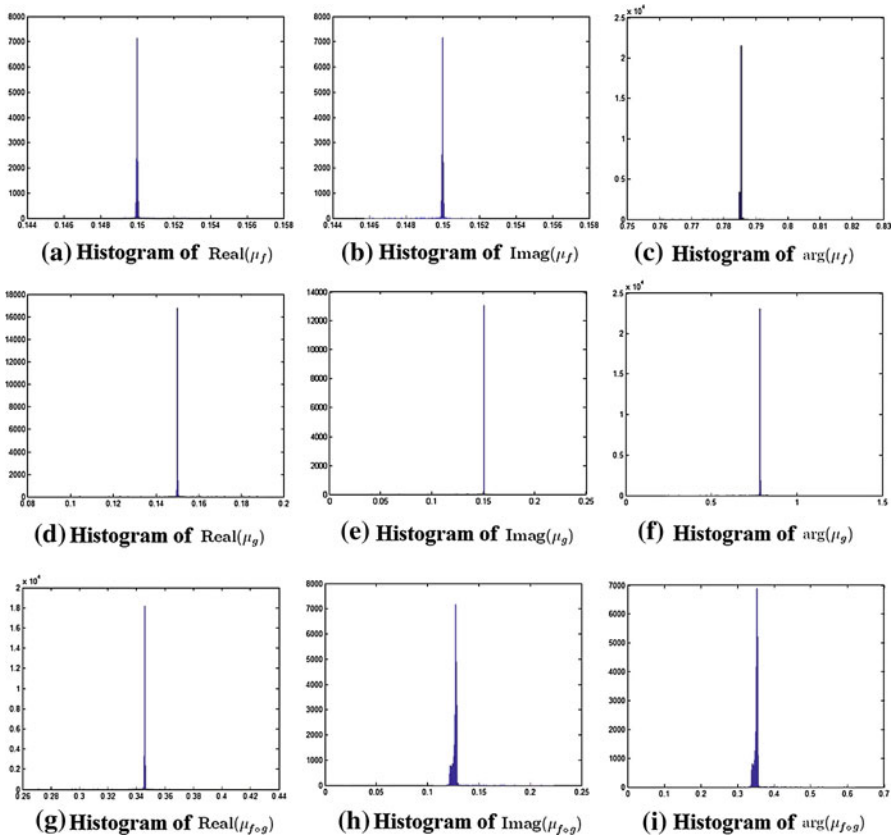


Fig. 11 Histogram of the real part, imaginary part and argument of the Beltrami coefficients

we compute a homology basis, $\{a, b\}$ as shown in the leftmost frame of the top row. We then embed a finite portion of the universal covering space of the Kitten model (as shown in Fig. 14) using the flat metric, shown in the right frame of the first row. The red rectangle shows the fundamental polygon, which is a parallelogram, with two adjacent edges z_a and z_b . The lattice Γ is formed by the translations generated by z_a and z_b ,

$$\Gamma = \{mz_a + nz_b | m, n \in \mathbb{Z}\}.$$

The Kitten surface can be represented as the quotient space $M = \frac{\mathbb{R}^2}{\Gamma}$. This gives the conformal parameter domain of the surface. The rightmost frame of the first row illustrates the circle packing texture mapping induced by the conformal parameterization. In the second and the third row, we set different Beltrami coefficients. $\mu(z)$ are constants for the second row. For the last row, the Beltrami coefficient is defined in a more complicated way. Because μ is defined on the Kitten surface, then it must satisfy the following consistency condition $\mu(z) = \mu(z + mz_a + nz_b)$. Given a point $z \in \mathbb{C}$, we

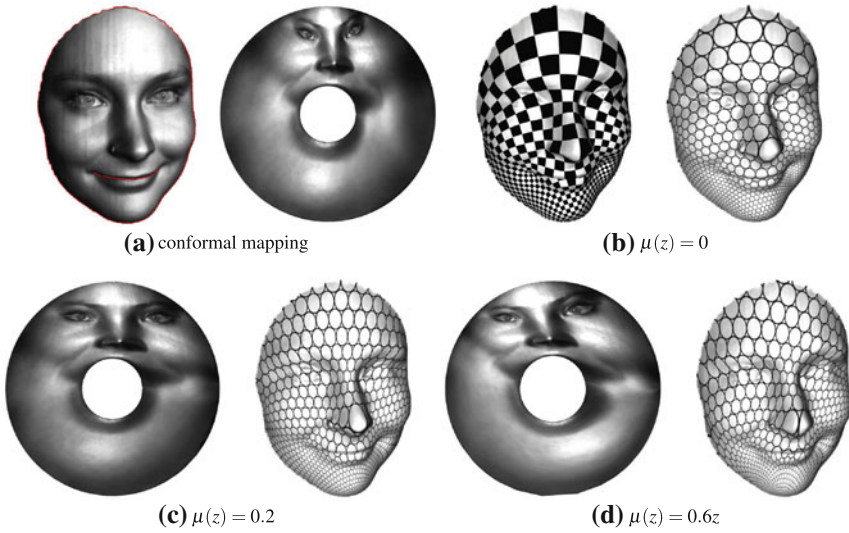


Fig. 12 Conformal and quasiconformal mappings for a topological annulus

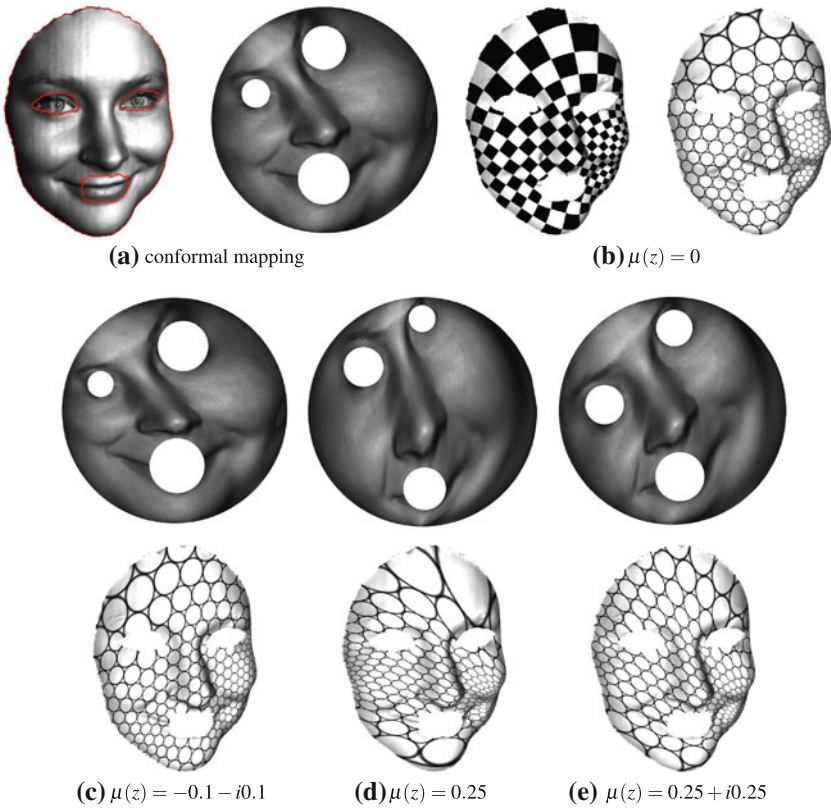


Fig. 13 Conformal and quasiconformal mappings for multiply connected domain

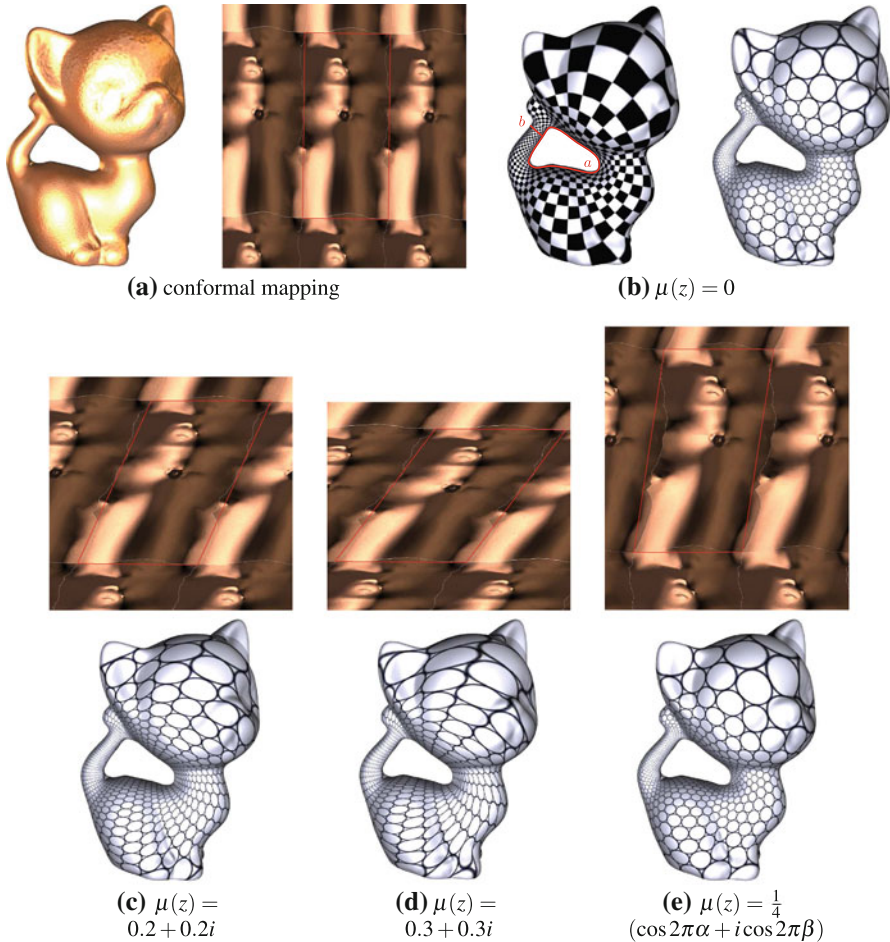


Fig. 14 Conformal and quasiconformal mappings for a genus one surface. The homology basis is $\{a, b\}$

can find a pair of real numbers $\alpha, \beta \in [0, 1)$, such that $z \equiv \alpha z_a + \beta z_b \pmod{\Gamma}$. Then μ is defined as $\mu(z) = \frac{1}{4}(\cos 2\pi\alpha + i \cos 2\pi\beta)$, which satisfies the above consistency condition.

7.6 Quasiconformal mappings for high genus surfaces

Our method can compute QC mappings for high genus surfaces, as shown in Fig. 15. We use hyperbolic Yamabe flow to compute the hyperbolic metric of the surface, then the homology basis $\{a_1, b_1, a_2, b_2\}$. We flatten a fundamental domain, compute the Fuchsian group generators, and flatten a finite portion of the universal covering space of the surface. Details can be found in [25,35]. This gives a conformal atlas of the surface. Because of the difference between hyperbolic metric and Euclidean metric, the texture mappings have seams in Fig. 15 along the homology basis. Also, the fundamental domains are color encoded in Fig. 15. Each connected domain sharing the same

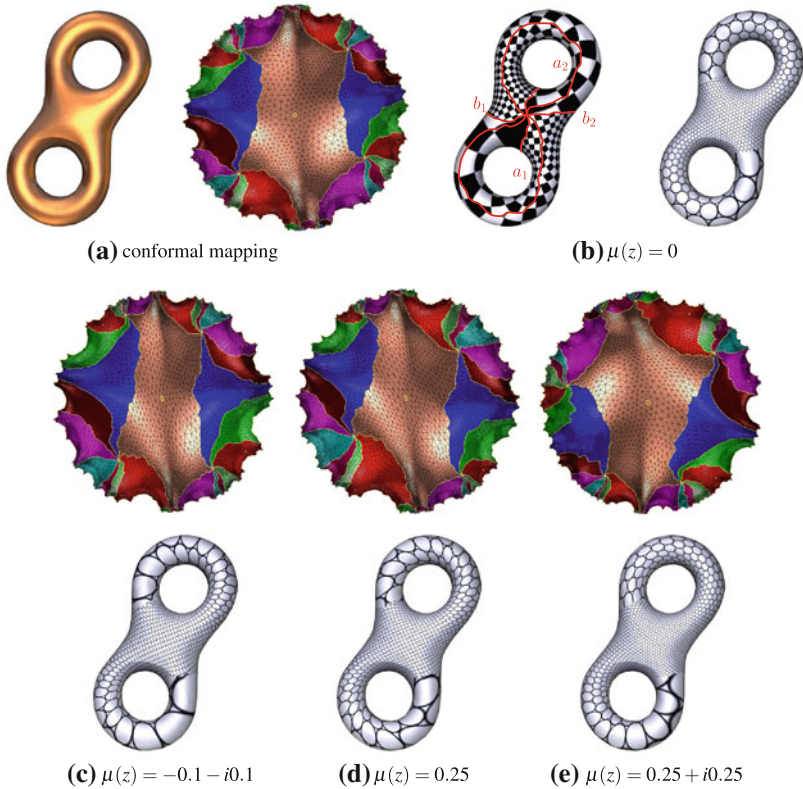


Fig. 15 Conformal and quasiconformal mappings for a genus two surface. The homology basis is $\{a_1, b_1, a_2, b_2\}$

color represents one fundamental domain. Suppose z and w are two local parameters, differ by a Möbius transformation, then μ should satisfy the following consistency relation (See Definition 4.5):

$$\mu(w) \frac{\bar{w}_z}{w_z} = \mu(z).$$

For example, let $p \in S$ is a point on a_k $p \in a_k$, it has two parameters $z_p \in a_k^+$ and $w_p \in a_k^-$, $w_p = \alpha_k(z_p)$. Then $\mu(z_p)$ and $\mu(w_p)$ should satisfy the above consistent constraint. In our experiments, we find a n -ring neighbor ($n = 4$) of a_k, b_k , denoted as R , then define $\mu(v_i) = z_0$ for all vertices v_i not in R , $\mu(v_i) = 0$, for v_i in a_k or b_k . μ is extended to other vertices as a complex valued harmonic function, $\Delta\mu(v_i) = 0$, $v_i \notin R \cup a_k \cup b_k$, where Δ is the Laplace–Beltrami operator of the original surface. This will ensure the consistency relation holds for μ . In Fig. 15, z_0 is $0.2 + i0.2$ for the left frame of second row, 0.3 for the right frame of the second row, and $z_0 = z$ for the last row. From the figure, we can see the deformation of the conformal structure of the surface (shape of the fundamental domain) with different Beltrami coefficients.

Table 3 Convergence Error of Mappings (E_z) and Beltrami Coefficients (E_μ): computing quasiconformal mappings for $n \times n$ grid meshes under different diffeomorphism transformations F with explicit Beltrami coefficients μ

Function	Error	$n = 10$	$n = 50$	$n = 100$	$n = 150$	$n = 200$	Conv. order
F_1	E_z	0.000272	0.000012	0.000006	0.000006	0.000006	1.1396
	E_μ	0.023638	0.004041	0.002342	0.001798	0.001956	0.85094
F_2	E_z	0.000537	0.000022	0.000009	0.000007	0.000007	1.3452
	E_μ	0.043494	0.007989	0.004008	0.002554	0.001994	1.0162
F_3	E_z	0.008977	0.000223	0.000056	0.000026	0.000015	2.0106
	E_μ	0.073561	0.012608	0.006268	0.004174	0.003148	1.055
F_4	E_z	0.001249	0.00005	0.000013	0.000006	0.000004	1.9343
	E_μ	0.081640	0.017682	0.008950	0.005994	0.004484	0.97429

The results show that our method can be applied effectively on general Riemann surfaces of high genus.

7.7 Numerical convergency analysis

We test the Quasi-Yamabe method on 4 diffeomorphisms with explicit formula and known Beltrami coefficients. These diffeomorphisms map the unit square to rectangles. For example,

$$F_1 = [f(x), f(y)], f(x) = \frac{\pi \times x + \cos(x \times \pi/2)}{\pi + 1},$$

$$F_2(x, y) = [f(x), g(y)], f(x) = \frac{\pi \times x + \sin(x \times \pi/2)}{\pi + 1}, g(y) = \frac{\pi \times y + \cos(y \times \pi/2)}{\pi + 1}.$$

Table 3 shows the error in the coordinates E_z and the error in the Beltrami coefficients E_μ , under the approximation of different meshes $n \times n$ with grid sizes $h = 1/n$. Specifically, E_z and E_μ are defined as: $E_z = \max\{|F_i - F_i^h|\}$ and $E_\mu = \max\{|\mu_{F_i} - \mu_{F_i^h}|\}$, where F_i^h is the approximation of F_i with mesh size h . E_z and E_μ both get smaller as the mesh grid size reduces. It illustrates that the discrete QC mapping converges to the continuous solution as $h \rightarrow 0$. We also computed the order of convergence by calculating the linear slope of $\log(E_z)$ and $\log(E_\mu)$ vs $\log(h)$. The order of convergence for E_z is greater than 1 in all cases, whereas the order of convergence for E_μ is greater than 0.5.

8 Conclusion

Many surface mappings are QC in the real world. According to QC Teichmüller theory, in general, there exists a one-to-one mapping between the QC mappings and the Beltrami coefficients. This work introduces a novel method to compute the *quasiconformal mapping* from the Beltrami differentials using the *auxiliary metric* method for *general Riemann surfaces*. The auxiliary metric is constructed from the Beltrami differential,

such that the desired QC mapping becomes a conformal one under the auxiliary metric. We present the discrete analogue of QC geometry on discrete triangular meshes using the discrete auxiliary metric. The discrete QC mapping is computed based on the discrete *Quasi-Yamabe flow*. Experimental results demonstrate the generality and accuracy of the proposed algorithm. The convergence of the QC mapping to the continuous solution as mesh grid size approaches to 0 is verified both theoretically and numerically. To the best of our knowledge, it is the first work to present the solution of surface QC mapping by solving the Beltrami equation using the auxiliary metric idea. This can also be applied to all conformal mapping methods.

References

1. Ahlfors, L.: Conformality with respect to Riemannian matrices. *Ann. Acad. Sci. Fenn. Ser.* **206**, 1–22 (1955)
2. Ahlfors, L.: *Lectures in Quasiconformal Mappings*. Van Nostrand Reinhold, New York (1966)
3. Ben-Chen, M., Gotsman, C., Bunin, G.: Conformal flattening by curvature prescription and metric scaling. *Comput. Graph. Forum* **27**(2), 449–458 (2008)
4. Bers, L., Nirenberg, L.: *On Linear and Nonlinear Elliptic Boundary Value Problems in the Plane*. pp. 141–167. *Convegno Internazionale Suelle Equazione Cremonese*, Roma (1955)
5. Bers, L.: *Mathematical Aspects of Subcritical and Transonic Gas Dynamics*. Wiley, New York (1958)
6. Bers, L.: Quasiconformal mappings, with applications to differential equations, function theory and topology. *Am. Math. Soc. Bull.* **83**(6), 1083–1100 (1977)
7. Bers, L., Nirenberg, L.: *On a Representation Theorem for Linear Elliptic Systems with Discontinuous Coefficients and its Applications*. pp. 111–140. *Convegno Internazionale Suelle Equazione Cremonese*, Roma (1955)
8. Bobenko, A., Springborn, B., Pinkall, U.: *Discrete conformal equivalence and ideal hyperbolic polyhedra* (2012, in press)
9. Bobenko, A.I., Springborn, B.A.: Variational principles for circle patterns and koebe's theorem. *Trans. Am. Math. Soc.* **356**, 659–689 (2004)
10. Bowers, P.L., Hurdal, M.: Planar conformal mapping of piecewise flat surfaces. In: *Visualization and Mathematics III*, pp. 3–34. Springer, Berlin (2003)
11. Bucking, U.: *On existence and convergence of conformally equivalent triangle meshes for conformal mappings and regular lattices*. In: *Barrett Memorial Lectures (May 17–21, 2010)*
12. Belinskii, P.P., Godunov, S.K., Yanenko, I.: The use of a class of quasiconformal mappings to construct difference nets in domains with curvilinear boundaries. *USSR Comp. Math. Phys.* **15**, 133–144 (1975)
13. Carleson, L., Gamelin, T.: *Complex Dynamics*. Springer, New York (1993)
14. Chow, B.: The Ricci flow on the 2-sphere. *J. Differ. Geom.* **33**(2), 325–334 (1991)
15. Chow, B., Luo, F.: Combinatorial Ricci flows on surfaces. *J. Differ. Geom.* **63**(1), 97–129 (2003)
16. Dai, J., Luo, W., Jin, M., Zeng, W., He, Y., Yau, S.T., Gu, X.: Geometric accuracy analysis for discrete surface approximation. *Comput. Aided Geom. Des.* **24**(6), 323–338 (2007)
17. Daripa, P.: On a numerical method for quasiconformal grid generation. *J. Comput. Phys.* **96**, 229–236 (1991)
18. Daripa, P.: A fast algorithm to solve nonhomogeneous Cauchy-Riemann equations in the complex plane. *SIAM J. Sci. Stat. Comput.* **13**(6), 1418–1432 (1992)
19. Daripa, P., Masha, D.: An efficient and novel numerical method for quasiconformal mappings of doubly connected domains. *Numer. Algorithm* **18**, 159–175 (1998)
20. Desbrun, M., Meyer, M., Alliez, P.: Intrinsic parameterizations of surface meshes. *Comput. Graph. Forum (Proc. Eurographics 2002)* **21**(3): 209–218 (2002)
21. Farkas, H.M., Kra, I.: *Riemann Surfaces*. Springer, Berlin (2004)
22. Floater, M.S., Hormann, K.: Surface parameterization: a tutorial and survey. In: *Advances in Multi-resolution for Geometric Modelling*, pp. 157–186. Springer, Berlin (2005)
23. Gortler, S.J., Gotsman, C., Thurston, D.: Discrete one-forms on meshes and applications to 3D mesh parameterization. *Comput. Aided Geom. Des.* **23**(2), 83–112 (2005)

24. Gotsman, C., Gu, X., Sheffer, A.: Fundamentals of spherical parameterization for 3D meshes. *ACM Trans. Graph.* **22**(3), 358–363 (2003)
25. Grimm, C., Hughes, J.F.: Parameterizing N-holed tori. In: *IMA Conference on the Mathematics of Surfaces*, pp. 14–29 (2003)
26. Grotzsch, H.: Über die verzerrung bei schlichten nichtkonformen abbildungen und eine damit zusammenhangende erweiterung des picardschen. *Rec. Math.* **80**, 503–507 (1928)
27. Gu, X., He, Y., Qin, H.: Manifold splines. *Graph. Models* **68**(3), 237–254 (2006)
28. Gu, X., Wang, Y., Chan, T.F., Thompson, P.M., Yau, S.T.: Genus zero surface conformal mapping and its application to brain surface mapping. *IEEE Trans. Med. Imaging* **23**(8), 949–958 (2004)
29. Gu, X., Yau, S.T.: Global conformal parameterization. In: *Symposium on Geometry Processing*, pp. 127–137 (2003)
30. Guggenheimer, H.W.: *Differential Geometry*. Dover Publications, New York (1977)
31. Hamilton, R.S.: Three manifolds with positive Ricci curvature. *J. Differ. Geom.* **17**, 255–306 (1982)
32. Hamilton, R.S.: The Ricci flow on surfaces. *Math. Gen. Relativ.* **71**, 237–262 (1988)
33. Hong, W., Gu, X., Qiu, F., Jin, M., Kaufman, A.E.: Conformal virtual colon flattening. In: *Symposium on Solid and Physical Modeling*, pp. 85–93 (2006)
34. Hormann, K., Levy, B., Sheffer, A.: Mesh parameterization. *SIGGRAPH 2007 Course Notes 2* (2007)
35. Jin, M., Kim, J., Luo, F., Gu, X.: Discrete surface Ricci flow. *IEEE Trans. Vis. Comput. Graph.* **14**(5), 1030–1043 (2008)
36. Kharevych, L., Springerborn, B., Schröder, P.: Discrete conformal mappings via circle patterns. *ACM Trans. Graph.* **25**(2), 412–438 (2006)
37. Kalberer, F., Nieser, M., Polthier, K.: Quadcover—surface parameterization using branched coverings. *Comput. Graph.* **26**(3), 375–384 (2007)
38. Lavrentjev, M.: Sur une classe de representations continues. *Rec. Math.* **48**, 407–423 (1935)
39. Lehto, O., Virtanen, K.: *Quasiconformal Mapping in the Plane*. Springer, Berlin (1973)
40. Lévy, B., Petitjean, S., Ray, N., Maillot, J.: Least squares conformal maps for automatic texture atlas generation. *SIGGRAPH 2002* pp. 362–371 (2002)
41. Lipman, Y., Chen, X., Daubechies, I., Funkhouser, T.: Symmetry factored embedding and distance. *ACM Trans. Graph.* **29**(4), 1–12 (2010)
42. Lui, L., Wong, T., Gu, X., Thompson, P., Chan, T., Yau, S.: Compression of surface diffeomorphism using Beltrami coefficient. *IEEE Comput. Vis. Patt. Recogn. (CVPR)*, pp. 2839–2846 (2010)
43. Lui, L., Wong, T., Gu, X., Thompson, P., Chan, T., Yau, S.: Hippocampal shape registration using Beltrami holomorphic flow. *Medical Image Computing and Computer Assisted Intervention (MIC-CAI)*, Part II. *LNCS 6362*, pp. 323–330 (2010)
44. Lui, L., Wong, T., Zeng, W., Gu, X., Thompson, P., Chan, T., Yau, S.: Detecting shape deformations using Yamabe flow and Beltrami coefficients. *J. Inverse Probl. Imaging (IPI)* **4**(2), 311–333 (2010)
45. Lui, L., Wong, T., Zeng, W., Gu, X., Thompson, P., Chan, T., Yau, S.: Optimization of surface registrations using Beltrami holomorphic flow. *J. Scientific Comput.* (2011)
46. Luo, F.: Combinatorial Yamabe flow on surfaces. *Commun. Contemp. Math.* **6**(5), 765–780 (2004)
47. Mastin, C., Thompson, J.: Discrete quasiconformal mappings. *Z. Angew. Math. Phys.* **29**, 1–11 (1978)
48. Mastin, C., Thompson, J.: Quasiconformal mappings and grid generation. *SIAM J. Sci. Stat. Comput.* **5**(2), 305–310 (1984)
49. Morrey, C.: On the solutions of quasi-linear elliptic differential equations. *Trans. Am. Math. Soc.* **43**, 126–166 (1938)
50. Praun, E., Hoppe, H.: Spherical parametrization and remeshing. *ACM Trans. Graph.* **22**(3), 340–349 (2003)
51. Ray, N., Li, W.C., Levy, B., Sheffer, A., Alliez, P.: Periodic global parameterization. *ACM Trans. Graph.* **25**(4), 1460–1485 (2005)
52. Sheffer, A., Lévy, B., Mogilnitsky, M., Bogomyakov, A.: ABF++: fast and robust angle based flattening. *ACM Trans. Graph.* **24**(2), 311–330 (2005)
53. Sheffer, A., Praun, E., Rose, K.: Mesh parameterization methods and their applications. *Foundations and Trends® in Computer Graphics and Vision* (2012, in press)
54. Sheffer, A., de Sturler, E.: Parameterization of faced surfaces for meshing using angle based flattening. *Eng. Comput.* **17**(3), 326–337 (2001)
55. Springerborn, B., Schröder, P., Pinkall, U.: Conformal equivalence of triangle meshes. *ACM Trans. Graph.* **27**(3), 1–11 (2008)

56. Vlasyuk, A.: Automatic construction of conformal and quasiconformal mapping of doubly connected and triple connected domains. *Akad. Nauk Ukrainy Inst. Mat., preprint (Akademiya Nauk Ukrainy Institut Matematiki, preprint)* **57**, 1–57 (1991)
57. Wang, S., Wang, Y., Jin, M., Gu, X.D., Samaras, D.: Conformal geometry and its applications on 3D shape matching, recognition, and stitching. *IEEE Trans. Pattern Anal. Mach. Intell.* **29**(7), 1209–1220 (2007)
58. Weisel, J.: Numerische ermittlung quasikonformer abbildungen mit finiten elementen. *Numer. Math.* **35**, 201–222 (1980)
59. Zayer, R., Levy, B., Seidel, H.P.: Linear angle based parameterization. In: *Symposium on Geometry Processing*, pp. 135–141 (2007)
60. Zeng, W., Jin, M., Luo, F., Gu, X.: Computing canonical homotopy class representative using hyperbolic structure. In: *IEEE International Conference on Shape Modeling and Applications (SMI 2009)* (2009)
61. Zeng, W., Marino, J., Gurijala, K., Gu, X., Kaufman, A.: Supine and prone colon registration using quasi-conformal mapping. *IEEE Trans. Vis. Comput. Graph. (IEEE TVCG)* **16**(6), 1348–1357 (2010)
62. Zeng, W., Samaras, D., Gu, X.: Ricci flow for 3D shape analysis. *IEEE Trans. Pattern Anal. Mach. Intell.* **32**(4), 662–677 (2010)
63. Zeng, W., Zeng, Y., Wang, Y., Yin, X., Gu, X., Samaras, D.: 3D non-rigid surface matching and registration based on holomorphic differentials. In: *The 10th European Conference on Computer Vision (ECCV) 2008*, pp. 1–14 (2008)